AD-A117 723 LA JOLLA INST CA F/G 20/14
PATH INTEGRAL FORMATION OF WAVE PROPAGATION IN THE IONOSPHERE, --ETC(U)
1982 V SESHADRI, B J WEST AFOSR-80-0187
UNCLASSIFIED LJI-R-82-195 AFOSR-TR-82-0578 NL

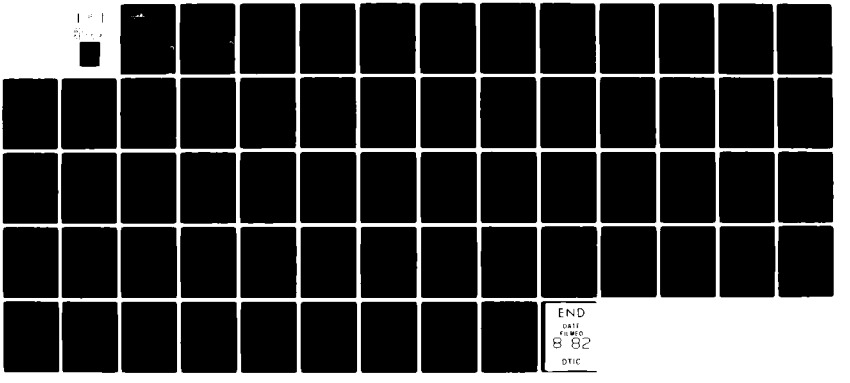

END
DATE FILMED
8 82
DTIC

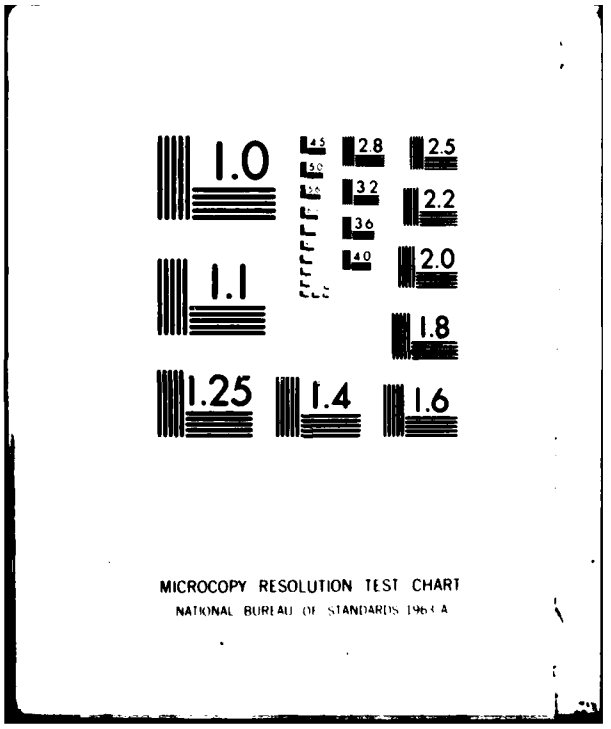
1.0
1.1
1.25
1.4
1.6
1.8
2.0
2.2
2.5
2.8
3.2
3.6
4.0
MICROCOPY RESOLUTION TEST CHART
NATIONAL BUREAU OF STANDARDS 1963 A

AFOSR-TR- 82-0578

(4)

LaJolla INSTITUTE

LJI-R-82-195

P.O. BOX 1434 • LA JOLLA • CALIFORNIA 92038 • PHONE (714) 454-6128



# PATH INTEGRAL FORMATION OF WAVE PROPAGATION IN THE IONOSPHERE: IV FINAL REPORT

V. SESHADRI

AND

BRUCE J. WEST

CENTER FOR STUDIES OF NONLINEAR DYNAMICS

LA JOLLA INSTITUTE
P.O. BOX 1434
LA JOLLA, CA 92038



SUPPORTED BY THE AIR FORCE OFFICE OF SCIENTIFIC RESEARCH

Unclassified

SECURITY CLASSIFICATION OF THIS PAGE (When Data Entered)

| REPORT DOCUMENTATION PAGE | READ INSTRUCTIONS BEFORE COMPLETING FORM |
|---|---|
| 1. REPORT NUMBER: AFOSR-TR- 82-0578 | 2. GOVT ACCESSION NO.: AD-A117 723 |
| | 3. RECIPIENT'S CATALOG NUMBER: |
| 4. TITLE (and Subtitle): Path Integral Formation of Wave Propagation In the Ionosphere IV | 5. TYPE OF REPORT & PERIOD COVERED: Final |
| | 6. PERFORMING ORG. REPORT NUMBER: |
| 7. AUTHOR(s): V. Seshadri and Bruce J. West | 8. CONTRACT OR GRANT NUMBER(s): AFOSR-80-0187 |
| 9. PERFORMING ORGANIZATION NAME AND ADDRESS: Center for Studies of Nonlinear Dynamics, La Jolla Institute, P.O. Box 1434, La Jolla, CA 92038 | 10. PROGRAM ELEMENT, PROJECT, TASK AREA & WORK UNIT NUMBERS: 61102F, 2310/A2 |
| 11. CONTROLLING OFFICE NAME AND ADDRESS: Air Force Office of Scientific Research/NC, Bldg 410, Bolling AFB, D. C. 20332 | 12. REPORT DATE: 1982 |
| | 13. NUMBER OF PAGES: 61 |
| 14. MONITORING AGENCY NAME & ADDRESS(if different from Controlling Office) | 15. SECURITY CLASS. (of this report): Unclassified |
| | 15a. DECLASSIFICATION/DOWNGRADING SCHEDULE: |

16. DISTRIBUTION STATEMENT (of this Report)
Approved for public release; distribution unlimited

17. DISTRIBUTION STATEMENT (of the abstract entered in Block 20, if different from Report)



18. SUPPLEMENTARY NOTES

19. KEY WORDS (Continue on reverse side if necessary and identify by block number)
Wave propagation
Born approximation
Rytev approximation
Scintillation
Scattering theory
Ionosphere

20. ABSTRACT (Continue on reverse side if necessary and identify by block number)
The validity of the application of weak scatter theory to ionospheric scattering data has been examined. It is concluded that the weak scatter theory is not universally applicable. Born and Rytov weak scatter calculations are compared and the Rytov calculations is found superior. The Rytov calculations appear to explain the enhancement in the scintillation index (the ratio on the intensity variance to variance of phase) in the equatorial vis a vis the polar stations. This research effort will be completed under Contract Number 49620-82-C-0058.

DD FORM 1 JAN 73 1473

Unclassified

SECURITY CLASSIFICATION OF THIS PAGE (When Data Entered)

LJI-R-82-195

# PATH INTEGRAL FORMATION OF WAVE PROPAGATION IN THE IONOSPHERE: IV FINAL REPORT

V. SESHADRI

AND

BRUCE J. WEST

CENTER FOR STUDIES OF NONLINEAR DYNAMICS

LA JOLLA INSTITUTE
P.O. BOX 1434
LA JOLLA, CA 92038

SUPPORTED BY THE AIR FORCE OFFICE OF SCIENTIFIC RESEARCH

## TABLE OF CONTENTS

ABSTRACT

We examine the validity of the application of weak scatter theory to ionospheric scattering data. We conclude that the weak scatter theory is not universally applicable. We also compare Born and Rytov weak scatter calculations and find the latter superior. The Rytov calculations also appear to explain the enhancement in the scintillation index $S_4/\sigma_\phi$ in the equatorial vis a vis the polar stations.

## 1. INTRODUCTION

Random fluctuations or scintillations of the phase and amplitude of electromagnetic signals propagating through the ionosphere have been observed experimentally. These signal fluctuations are attributed primarily to the fluctuations in the plasma density in the F-layer of the ionosphere and depend on such factors as the wavelength of the signal, the source-receiver geometry, the geo-physical conditions, etc. In the past two decades both in situ and remote observations have been made to elucidate the morphological properties of irregularities causing the scintillation. The earliest observations of the scintillations involved radio emissions from stellar sources[1]. These scintillations were later identified as originating in the ionosphere[2]. Booker[3] has made a detailed review of the radio star observations. With the advent of satellites, controlled experiments could be performed. Yeh and Swenson[4] have reviewed the early satellite measurements. In the mid- and late seventies wide band satellites in polar orbits were launched and a vast amount of detailed information gathered[5-13]. Particularly relevant to this report are the data obtained from the U.S. Navy Navigational Systems satellites[6,7] and the Air Force P76-5 wideband satellite[9-13].

Theoretical analysis of the scintillation problem has been carried out by several authors. Booker et al.[14] proposed that the diffraction of the radio waves by the fluctuations in electron density in the ionosphere could cause the observed scintillation. They modeled the effect of the electron density fluctuations by a thin phase changing diffraction screen. Further work on the phase screen model was carried out by Mercier[15] and Briggs and Parkin[16]. The scintillation problem has also been analyzed using the weak scintillation models developed by researchers in other fields (see, for example, the monograph of Tatarski [17]). Under weak scintillation, either the

Born approximation or the Rytov approximation solution to the scalar wave equation is applicable. Crane [6,7] and Rino[12] and Fremouw[13] have used such weak scatter formulas to analyze the satellite data. Strong scatter theories have been developed, among others, by Prokhorov et al.[18], Fante[19], Ishimaru[20] and Rumsey[21]. Recently, Dashen[22,23] has developed a path integral formulation of the problem.

These above mentioned approaches can be used to yield such measures of scintillation as, the variance of phase $\langle \phi^2 \rangle$,† the variance of amplitude $\langle \chi^2 \rangle$, variance of intensity $S_4$, scintillation index $S_4/\langle \phi^2 \rangle$, etc. These are basically various types of moments of the distribution function of the electric field. To date, there has been no satisfactory prediction of the distribution of the field for a general ionospheric scattering situation. For a weak scintillation, an argument based on the central limit theorem has been advanced which yields Gaussian distributions for the in-phase and quadrature components of the electric field in the Born approximation[24] and for the phase and log-amplitude in the Rytov approximation[17]. Crane[6,7] has argued that the use of the central limit theorem cannot be justified for what amounts to single scattering approximations. In any event, the log-normal distribution does not appear to fit the ionospheric data well. For practical data analysis the Nakagami-m distribution appears to be useful[10,25]. The Nakagami-m model is restricted to the description of intensity statistics and provides an intensity distribution function which reduces in the appropriate limits to the Rice Distribution and the Rayeligh Distribution, respectively. Fremouw et al.[10] have recently proposed a two-component model in which the electric field is

† The brackets denote an average over the plasma fluctuations.

modeled as the product of a diffractively scattered component $E_s \equiv X_s + iY_s$ and a refractively focused component $E_f \equiv \exp[X_f + i\Phi_f]$. $X_s$, $Y_s$, $X_f$ and $\Phi_f$ are assumed to be Gaussian and $E_s$ is uncorrelated with $E_f$. This model requires six independent parameters, which must be found from the data, for a complete description.

The purpose of this final report is to examine the compatibility of the ionospheric data with the various theoretical approximations. The ionospheric scattering is quite complicated because of the anisotropy of the irregularities, the power-law spectrum of scales in the plasma fluctionas and the source motion. These factors, coupled with the data processing constraints, prevent a single viable theoretical approach for the entire satellite pass. Unlike the conclusion of Rino[12], in most cases, the scattering cannot be determined to be weak for an entire pass. Most data show intense scintillations for at least a portion of the pass, particularly in the auroral region. Hence, a strong scatter theory has to be used in these regions. Also, in agreement with Crane's analysis[6,7], the Rytov approximation is preferable to the Born approximation, particularly in the equatorial region.

In Section 2, we briefly review the literature on the ionospheric scattering. Section 3 contains an analysis of the Rytov approximation. In Section 4, the Rytov and Born results for a number of satellite pass configurations are compared and are shown to be significantly different. Complete passes both for equatorial and polar stations are calculated in the Rytov approximation and the validity of this approximation is discussed. Section 5 reiterates some of the important conclusions.

## 2. A REVIEW OF IONOSPHERIC SCINTILLATION THEORIES AS APPLIED TO THE SATELLITE DATA

### (i) Helmholtz and Parabolic Equations

Ionospheric scintillation is caused by electron density irregularities which act at fluctuations in the refractive index for the electromagnetic wave[14]. A complete theory for wave propagation through a medium with random variations in the refractive index is not available but approximate solutions can be sought in the various parameter domains. Development of these approximate solutions has been initiated in such related fields as optical propagation through the atmosphere[17], acoustical propagation in the ocean[23], radiowave transmission through the ionosphere, etc. The work prior to 1970 is reviewed in the article of Barbanenkov et al.[26]. The work carried out in the 70's is reviewed by such authors as Fante[19], Prokhorov et al.[18], and Crane[7]. The path integral formulation of the signal propagation in random media is reviewed in a book by Flatté et al.[23]. Applications of these theories specifically to the inospheric scattering have been carried out by Crane[6,7], Fremouw et al.[9-13], Rino et al.[9-13] and Seshadri and West[27].

The usual starting point for the analysis of the effects of a random refractive index on the propagation of scalar waves is the scalar wave equation. The use of the scalar wave equation to describe the propagation of electromagnetic waves in the presence of a wide range of refractive index fluctuations cannot be justified a priori. However, the investigation of the polarization effects in the vector Helmholtz equation indicates that for irregularities in the far field of both the source and the receiver and possessing scales $L \gg \lambda$ the wavelength of propagation, the depolarization effect is second order and may be neglected[28,29]. Booker and Ferguson[30] have inferred that the inner scale cut-off is approximately the ion gyro radius, $\sim$5m. From these considerations,

the scalar wave equation should prove adequate for the largest wavelengths of interest (of the order of 3m), and the polarization effects should prove negligible.

The scalar wave equation for the wave amplitude $\Psi(\underline{r},z,t)$ is given by

$$\nabla^2\Psi(\underline{r},z,t)-\frac{1}{c^2}\frac{\partial^2\Psi}{\partial t^2}(\underline{r},z,t) = 0 \qquad (2.1)$$

where $\underline{r} = (x,y)$ are the transverse coordinates and z is in the direction of propagation. Assuming a solution of the form

$$\Psi(\underline{r},z,t) = \mathrm{Re}\left\{E(\underline{r},z,t)\, e^{i(kz-\omega t)}\right\} \qquad (2.2)$$

and substituting (2.2) into (2.1) one obtains the Helmholtz equation

$$\nabla^2E(\underline{r},z,t) + k^2n^2(\underline{r},z,t)E(\underline{r},z,t) = 0\,. \qquad (2.3)$$

The quantity $n(\underline{r},z,t)$ is the refractive index of the medium, which in the case of the ionosphere, is a random function of position due to the presence of electron density irregularities.

The Helmholtz equation (2.3) is an elliptic partial differential equation, so that in order to find the electric field at a given spatial point one must solve the equation for the field at all points in space. This property limits the analytical and numerical tractability of (2.3). In the weak scintillation case, perturbative solutions such as the Born and Rytov approximations can be obtained from the Helmholtz equation. In the strong scintillation case the Helmholtz equation is first approximated by the parabolic equation; (we will presently give a mathematical definition of weak and strong scintillation)

$$2ki\,\frac{\partial}{\partial z}\,E(\underline{r},z,t|\underline{r}_o,0)+\left\{\nabla^2_{\underline{r}} + 2k^2[n^2(\underline{r},z,t)-1]\right\} E(\underline{r},z,t|\underline{r}_o,0) = 0, \qquad (2.4)$$

where $\nabla^2_{\underline{r}} = \frac{\partial^2}{\partial x^2} + \frac{\partial^2}{\partial y^2}$.

This equation is the starting point of the moment analysis of such authors as Barbenenkov et al.[26], Tatarski[17], Taylor[31], de Wolf[32] and Rumsey[21]. It is also the starting equation for Dashen's path integral formulation[22,23]. In the parabolic approximation, the normal to the wave front of the electric field is assumed to remain close to the z-axis and the field is assumed to obey the boundary condition

$$\lim_{z\to 0} E(\underline{r},z|\underline{r}_o,0) \to \left(\frac{k}{2i\pi z}\right) e^{ik(\underline{r}-\underline{r}_o)^2/2z} \quad . \qquad (2.5)$$

The square of the refraction index $n^2(\underline{r},z,t)$ is a product of the dielectric coefficient $\varepsilon(\underline{r},z,t)$ and the magnetic permeability of the medium. When the medium is turbulent, as in the case of the ionosphere, the refractive index is a fluctuating quantity. The magnetic permeability is usually assumed to be constant and set equal to its vacuo value of unity. The dielectric coefficient $\varepsilon(\underline{x},t)$, a random function of $\underline{x} \equiv (\underline{r},z)$ and t, is defined in terms of its statistical properties. The average value of $\varepsilon(\underline{x},t)$, where the average is performed over an ensemble of realizations of the plasma fluctuations, can, without loss of generality, be set equal to unity. Thus, one can partition $\varepsilon(\underline{x},t)$ as a sum of its average value and the fluctuations $\mu(\underline{x},t)$ about this average, i.e.,

$$\varepsilon(\underline{x},t) = 1 + \mu(\underline{x},t) \qquad (2.6)$$

where, by definition, indicating the average by a bracket, we have

$$\langle\mu(\underline{x},t)\rangle = 0. \qquad (2.7)$$

The fluctuations $\mu(\underline{x},t)$ are further specified by their two-point correlation function $\rho$ as

$$\rho(\underline{x},\underline{x}',t,t') = \langle\mu(\underline{x},t)\ \mu(\underline{x}',t')\rangle\ . \tag{2.8}$$

For a stationary homogeneous medium, $\rho$ is a function only of the spatial difference $\underline{x}-\underline{x}'$ and time difference $t-t'$. Thus, assuming the ionosphere to have stationary and homogeneous fluctuations, we write the correlation function as[23]

$$\rho(\underline{x}-\underline{x}',t-t') = \langle\mu(\underline{x},t)\ \mu(\underline{x}',t')\rangle\ . \tag{2.9}$$

The fluctuations $\mu(\underline{x},t)$ are further assumed to have a power law spectrum, i.e., for small $\Delta\underline{x} = (\Delta x,\Delta y,\Delta z)$ and $\Delta t = (t-t')$, we expand $\rho(\Delta\underline{x},\Delta t)$ as

$$\rho(\Delta\underline{x},\Delta t) = \langle\mu^2\rangle\left(1-\left|\frac{\Delta z}{L_z}\right|^{p-1} - \left|\frac{\Delta x}{L_x}\right|^{q-1} - \left|\frac{\Delta y}{L_y}\right|^{b-1} - \left|\frac{\Delta t}{\tau}\right|^{w-1}\right) + \ldots \tag{2.10}$$

where p,q,s and w are the power law exponents and are in general unequal. For the ionosphere the quantities $L_z$, $L_x$, $L_y$ and $\tau$ can vary over a wide range depending on the properties of the scattering layer and the location and orientation of $\Delta\underline{x}$ with respect to the geomagnetic equator. A further restriction on $\mu(\underline{x},t)$ which is usually made is that it is either a Gaussian random field or that $kL_{max}\langle\mu^2\rangle^{1/2} \ll 1$[with $L_{max} = \max(L_z, L_x, L_y)$] in which case the distribution need not be specified[22].

The conditions for the validity of the parabolic equation (2.4) can be expressed in terms of the correlation length $L_{max}$ and the correlation time $\tau$[22]. The conditions are: (1) that the spatial scales for the fluctuations are very much greater than the wavelength of the source wave $kL_{max} \gg 1$; (2) $kL_{max} \ll \omega\tau$ ; and that (3) the root mean square (rms) multiple scattering angle should

be small, i.e., $[\langle\mu^2\rangle R/L_{max}]^{1/2} \ll 1$. Here, R is the total distance of propagation.

(ii) Characterization of the Scintillation

The scintillation characteristics of a wave propagating through a random medium can be described in terms of single point and multipoint functions. By a single point function we mean quantities that depend on the distribution of the electric field at a single point, e.g., quantities such as the mean and the variance of the phase or the amplitude. Multipoint functions such as correlation functions of the amplitude depend on the joint probability distribution of the electric field at more than one point. Single point functions are easier to evaluate than multipoint functions and provide useful guidelines for theoretical formulation of approximate solutions of the problem.

For an isotropic medium with a single scale, Tatarski[17] has introduced two parameters to quantitatively specify the saturation characteristics of the propagating wave in terms of the medium characteristics. The first parameter is the rms phase fluctuation as computed in first order geometric optics, i.e.,

$$\Phi^2 = k^2 \left\langle \left[ \int_0^R \mu(\underline{r},z,t)\, dz \right]^2 \right\rangle$$

$$= k^2 R \int_{-\infty}^{\infty} \rho(|z|, o)\, dz + O(L_z/R) \,. \qquad (2.11)$$

In (2.11), the direction of propagation has been taken to be along the z-axis. The parameter $\Phi$ is a measure of the strength of the phase fluctuations for a total propagation distance R. The second parameter, called the diffraction parameter (closely related to Tatarski's wave parameter), is the square of the ratio of the Fresnel zone size to the scale size L and is given by

$$\Lambda = R/5kL^2 \ . \qquad (2.12)$$

When $\Phi$ is less than unity, or less than $\Lambda^{-1}$, either geometric optics or the Rytov approximation is valid[23]. In this case, there is a simple relation between the statistics of $E(\underline{x},t)$ or of $\ell n\ E(\underline{x},t)$ and that of $\mu$. When both $\Phi$ and $\Lambda\Phi$ are greater than unity, the fluctuations in $E(\underline{x},t)$ saturate. In this case, the properties of $E(\underline{x},t)$ are governed by statistical considerations rather than by the detailed properties of $\mu$. The path integral formulation is particularly useful for moment calculations in this regime.

The scintillation characteristics can thus be summarized in the $\Lambda\Phi$ diagram as shown in Figure 1. There are three regions in this diagram and different theoretical approximations apply in each. In the geometrical optics region the Born approximation is adequate. When $\Lambda$ is larger than unity, the Rytov extension is adequate as long as $\Phi^2<1$. In the saturated region, multiple scattering effects have to be included. A thorough discussion of the statistical properties in the various scattering regimes with particular emphasis on the relation of these properties to the ray theory can be found in Dashen's article[22].

(iii) Scintillation Characteristics of Ionospheric Scattering

Characterizing the scintillation caused by ionospheric irregularities is complicated because of the presence of multiple scales[27C]. Further, the irregularities in the F-layer are highly anisotropic[6]. These two features play a crucial role in the overall scintillation behavior. Experimental evidence suggests that the ionospheric irregularities have a power law spectrum with spectral index $\nu<4$. The inner and outer scale cutoffs are not known precisely

but the latter is presumed to be quite large. The inner scale can usually be extended to zero without causing any major complication. Even with the knowledge of these two cutoffs, the precise form of the spectrum (it is a power law only asymptotically for large spatial frequencies) is not known. The anisotropy factors have been inferred from both remote and *in situ* measurements. In the equatorial region, the irregularities are aligned along the earth's magnetic field and are elongated along the field lines[2]. These are frequently referred to as being rod-like and can have elongation ratios of up to 100. In the auroral region there is considerable evidence that the irregularities are elongated along two axes and are sheet-like[9-13]. These anisotropy factors play a major role in the observed differences in the scintillation characteristics of the polar and equatorial regions.

Two additional factors that complicate ionospheric scintillation studies are the satellite motion and the nature of the data processing. The collection and processing of the wide-band satellite data is discussed in a series of reports and papers by Fremouw et al.[9-13]. Two points regarding the processing which are particularly relevant as far as this report is concerned are that 1) the raw data is subjected to a sharp cutoff high-pass filter with a cutoff frequency $\tau_c^{-1}$ and 2) the satellite data are analyzed in segments $\tau_D$, which are 20 to 80 seconds long. As pointed out by Fremouw and Rino, these two parameters play a decisive role in determining the rms phase[9-13].

The phase fluctuations are affected quite strongly by the large-scale spatial perturbations, and the outer scale cutoffs become quite important. This problem does not occur in the calculation of $\Lambda$ because Fresnel filtering effectively suppresses these large scales. For the phase fluctuations, however, the outer scale cutoffs are set either by the medium or by some measurement window. In the wide-band satellite measurements, the scale set by the

measurement window, which is much smaller than the actual outer scale of the ionosphere, is the relevant scale cutoff. This scale cutoff can be taken to be some effective length $L_e$ traversed by the satellite within the smaller of the two periods $\tau_c$ or $\tau_D$. Thus, the measured phase fluctuations depend on $L_e$, which is a product of either $\tau_c$ or $\tau_D$ and the effective velocity of the satellite with respect to the receiver. The effective velocity can be quite strongly dependent on the location of the receiver because of the anisotropy of the ionosphere. Fremouw[13] has argued that this variation of the effective velocity can explain the differences in the scintillation features observed between equatorial and polar stations.

The scale cutoff set by the measurement window does not significantly alter the amplitude or the intensity fluctuations because of Fresnel filtering but the phase variance is significantly altered. Because of the smaller effective length $L_e$, there is a significant difference in the results for the phase variance as computed in the Born approximation and the Rytov approximation. Rino and Fremouw[9-13] compute the phase in the Born approximation neglecting diffraction effects. It is shown in the next two sections that this can lead to a sighificant error for the phase, even when the overall scintillation is small.

## 3. THE FIRST BORN VS. THE RYTOV APPROXIMATION

Theoretical analysis of the wide-band satellite data has been carried out by several workers assuming that the scattering is weak and that the Born approximation is adequate[9-13]. In the computation of the variance of the phase in the Born approximation, the propagation effects are neglected. The result for $\langle \phi^2 \rangle$ is identical to that computed in a thin phase screen calculation[33]. The latter calculation can be carried out easily. The same quantity can also be computed in the Rytov approximation. These two results differ considerably for two typical satellite passes, over the equatorial and polar stations, respectively. To see the origin of these differences, we first compute the phase in the thin phase screen approximation.

The phase change induced by the plasma density fluctuations is given in the zeroth order approximation by the line integral[33]

$$\delta\phi = -r_e \lambda \int \Delta N_e(\underline{r}) d\ell \ , \tag{3.1}$$

where we have assumed that both the measurement frequency and the reference frequency are well above the plasma frequency, $r_e$ is the classical electron radius, $\lambda$ is the wavelength of the incident radiation, $\Delta N_e$ is the local electron density perturbation, and the line integral is along a straight line path from the source to the receiver. Let the layer thickness be $\Delta L$, $\theta$ be the direction of propagation with respect to the z-axis and $\hat{\underline{a}}_k$ be the unit vectors transverse to the direction of propagation for a receiver point with coordinates $(\underline{\rho},z)$ (See Figs. 2, 3). The line integral (3.1) can be written as

$$\delta\phi(\underline{\rho},z) = -r_e\lambda \sec\theta \int_0^{\Delta L} \Delta N_e(\underline{\rho} + \tan\theta \ \hat{\underline{a}}_k \ (\eta - z), \eta) d\eta . \tag{3.2}$$

Then by direct computation

$$R_{\delta\phi}(\underline{\rho}-\underline{\rho}') = \langle \delta\phi(\underline{\rho},z)\delta\phi(\underline{\rho}',z)\rangle$$

$$= r_e^2\lambda^2 \sec^2\theta\Delta L$$

$$\times \int_{-\Delta L}^{\Delta L} \left(1 - \frac{|\eta|}{\Delta L}\right) R(\underline{\rho}-\underline{\rho}'+\eta \tan\theta \ \hat{\underline{a}}_k, \eta)d\eta \qquad (3.3)$$

where $R(\underline{\rho},z)$ is the three-dimensional autocorrelation function of $\Delta N_e(\underline{r})$. Introducing the Fourier transform $F(\underline{k},k_z)$ of $R(\underline{\rho},z)$ as

$$R(\underline{\rho},z) = \frac{1}{(2\pi)^3}\iiint e^{i(\underline{k}\cdot\underline{\rho} + k_z z)}F(\underline{k},k_z)d^2k dk_z \qquad (3.4)$$

in (3.3) and performing the $\eta$ integration, we arrive at the result:

$$R_{\delta\phi}(\underline{\rho}-\underline{\rho}') = r_e^2\lambda^2 \sec^2\theta\Delta L$$

$$\times \frac{1}{(2\pi)^3}\iint d^2k e^{i\underline{k}\cdot(\underline{\rho}-\underline{\rho}')}\int dk_z \ F(\underline{k},k_z)$$

$$\times \int e^{i(\underline{k}\cdot\hat{\underline{a}}_k \tan\theta)\eta + ik_z\eta(1-|\eta|/\Delta L)}d\eta \ . \qquad (3.5)$$

Assuming that the correlation length $L_z$ along the z-direction is much shorter then the layer thickness, we can neglect the factor $|\eta|/\Delta L$ and take the limits of integration to $\infty$. The integration over $\eta$ then yields the $\delta$-function $2\pi\delta(k_z + \underline{k}\cdot\hat{\underline{a}}_k \tan\theta)$. Performing the $k_z$ integration then leads to the formulae

$$R_{\delta\phi}(\underline{\rho}-\underline{\rho}') = r_e^2 \sec^2\theta\Delta L \iint \frac{d^2k e^{i\underline{k}\cdot(\underline{\rho}-\underline{\rho}')}}{(2\pi)^2}F(\underline{k}, -\tan\theta \ \hat{\underline{a}}_k \cdot \underline{k}). \qquad (3.6)$$

When the cutoffs are imposed by the detrender the integration over the transverse spatial frequencies $\underline{k}$ must be carried out only over those spatial

frequencies $|\underline{k}| > k_e \sim 2\pi/L_e$. Thus, the cutoffs in the integration in (3.6) are not imposed solely by the medium but also by the nature of the data processing.

We proceed further by assuming the same functional form of $F(\underline{k},k_z)$ as that assumed by Rino and Fremouw[9-13]. They have shown that for a general anisotropy model[34] (Fig. 4)

$$F(\underline{k},-\tan\theta\ \hat{\underline{a}}_k \cdot \underline{k}) = ab \left\langle \Delta N_e^2 \right\rangle Q([\ Ak_x^2 + Bk_xk_y + Ck_y^2]^{\frac{1}{2}}) \tag{3.7}$$

where a and b are the axial ratios along the principal irregularity axes, respectively, and $k_x$, $k_y$ are x and y components of the transverse wave vector $\underline{k}$, respectively. The coefficients A, B, C depend on the propagation angle relative to the principal irregularity axis and are given in Eq. 41 of Ref. [24]. They have further assumed the following form for the spectral distribution function Q(q),

$$Q(q) = 8\pi^{3/2}\ \frac{\Gamma(\nu+1/2)}{\Gamma(\nu-1)}\ \frac{q_0^{2\nu-2}}{(q_0^2+q^2)^{\nu+\frac{1}{2}}}, \tag{3.8}$$

where $q_0$ is the outer scale cutoff wave number and $\nu$ is the spectral index of the power law. With the definition

$$C_s = 8\pi^{3/2}\left\langle \Delta N_e^2 \right\rangle q_0^{2\nu-2}\Gamma(\nu+1/2)/\Gamma(\nu-1) \tag{3.9}$$

we have

$$F(\underline{k},\ -\tan\theta\ \hat{\underline{a}}_k\cdot\underline{k}) = abC_s\ \frac{1}{(q_0^2+q^2)^{\nu+\frac{1}{2}}} \tag{3.10}$$

where $q^2 = Ak_x^2 + Bk_xk_y + Ck_y^2$. We now substitute (3.10) into (3.6) with the appropriate change of variables and an angular integration and arrive at the correlation function[27b]

$$R_{\delta\phi}(y) = r_e^2 \lambda^2 \Delta L \sec\theta \, GC_s \int \frac{qJ_0(qy)}{(q_0^2+q^2)^{\nu+1/2}} \frac{dq}{2\pi} \tag{3.11}$$

where

$$G = \frac{ab}{\sqrt{AC-B^2/4 \cos\theta}} ; \tag{3.12a}$$

$J_0$ is the Bessel function of order zero and

$$y = \left(C\rho_x^2 - B\rho_x\rho_y + A\rho_y^2\right)^{1/2} / \left(AC - B^2/4\right)^{1/2} . \tag{3.12b}$$

The main point now is the choice of the value of the cutoff that is to be imposed on the integration over the spectrum of plasma density fluctuations. We <u>assume</u> that the cutoff to be imposed, as far as the outer scale is concerned, is

$$q_e = \frac{2\pi}{L_e} \tag{3.13}$$

where the effective scale length $L_e$ is

$$L_e = V_e \tau_e \tag{3.14}$$

in terms of the effective velocity $V_e$

$$V_e = \left[\frac{C V_x^2 - BV_xV_y + AV_y^2}{AC - B^2/4}\right]^{1/2} \tag{3.15}$$

and $\tau_e \equiv \min(\tau_c, \tau_D)$. This assumption is motivated by the fact that the satellite samples fluctuations of the scale $L_e = V_e\tau_e$ only. Using this assumption

$$R_{\delta\phi}(y) = r_e^2\lambda^2\ \Delta L\ \sec\theta GC_s \int_{q_e}^{\infty} \frac{qJ_0(qy)}{(q_0^2+q^2)^{\nu+\frac{1}{2}}}\,\frac{dq}{2\pi} \tag{3.16}$$

It should be pointed out that this assumption is almost the same as the one made by Rino[12] and Fremouw[13]. Their formula involves dropping $q_0$ altogether in (3.16), a procedure which is valid when $q_0 << q_e$.

In ionospheric measurements, the receiver is fixed and phase fluctuations arising out of the satellite motion appear as temporal fluctuations. To convert (3.16) to a formula yielding temporal fluctuations we set $y = V_e t$, and

$$R_{\delta\phi}(V_e t) = r_e^2\lambda^2\ \ \Delta L\ \sec\theta\ \frac{GC_s}{2\pi} \int_{q_e}^{\infty} \frac{qJ_0(qV_e t)dq}{(q_0^2+q^2)^{\nu+\frac{1}{2}}}\ . \tag{3.17}$$

Let the measured phase fluctuation in a satellite pass be

$$\phi^2_{\tau_c} = \frac{1}{\tau_c}\int_0^{\tau_c} \phi^2(t')dt'. \tag{3.18}$$

An ensemble average of this quantity over an ensemble of statistically identical ionospheres is given by

$$\phi^2 = \Phi^2_{\tau_c} = \left\langle \phi^2_{\tau_c} \right\rangle\ . \tag{3.19}$$

The quantity $\Phi_{\tau_c}$ can be obtained from the correlation function (3.17) by setting t=0,[12] i.e.,

$$\phi^2_{\tau_c} = R_{\delta\phi}(0) = r_e^2\lambda^2\,\Delta L\,\sec\theta\,\frac{GC_s}{2\pi}\int_{q_e}^{\infty}\frac{q\,dq}{(q_0^2+q^2)^{\nu+\frac{1}{2}}}$$

$$= \frac{r_e^2\lambda^2\,\Delta L\,\sec\theta\;\;GC_s}{2\pi}\,\frac{1}{(2\nu-1)}\,\frac{1}{(q_0^2+q_e^2)^{\nu-\frac{1}{2}}} \quad . \tag{3.20}$$

The result (3.20) is the same as that obtained by Rino[12] if $q_0$ is set equal to zero, i.e., $q_0 << q_e$. However, if $q_e$ is comparable to $q_0$ the full expression for $\Phi_{\tau_c}$ must be used.

This result cannot be compared with the phase variance computed in the Rytov approximation. The Rytov approximation can be arrived at in a variety of fashions. One of the clearer presentations indicating the nature of the approximations involved is given in the report by Callan and Zachariasen[35,36]. The electric field is expressed as

$$E(\underline{R}) = E_0(\underline{R})e^{X(\underline{R})}, \tag{3.21}$$

where $E_0(\underline{R})$ is the unperturbed solution of the wave equation at $\underline{R}$ with a source at the origin, i.e.,

$$(\nabla^2 + q^2)E_0(\underline{r}) = \delta(\underline{r}), \text{ and}$$

$$E_0(\underline{r}) = \frac{e^{iq|\underline{r}|}}{4\pi|\underline{r}|} \quad . \tag{3.22}$$

The function $X(\underline{r})$ is given by

$$X(\underline{r}) = \frac{-4\pi r_e}{E_0(\underline{r})}\int d^3r' E_0(\underline{r}-\underline{r}')\Delta N_e(\underline{r}')E_0(\underline{r}'). \tag{3.24}$$

It may be seen from (3.24) that (3.21) can be obtained simply by exponentiating the perturbative term in the Born approximation.

All the quantities of interest for ionosphere scattering may be computed easily from (3.24). Let us first split the function X into real and imaginary parts:[36]

$$X = X_1 + iX_2 \ . \tag{3.25}$$

Then

$$E(\underline{R}) = E_0(\underline{R})e^{X_1(\underline{R}) + iX_2(R)} \ . \tag{3.26}$$

The perturbed phase $\phi(\underline{R})$ is then equal to $X_2(\underline{R})$. Thus,

$$\begin{aligned} \langle \phi^2 \rangle &= \left\langle X_2^2(\underline{R}) \right\rangle \\ &= \frac{1}{2}\left[ \left\langle |X|^2 \right\rangle - \mathrm{Re} \left\langle X^2 \right\rangle \right] \ . \end{aligned} \tag{3.27}$$

Similarly, the log-intensity $\chi$ can be defined

$$\chi \equiv \log |E(\underline{R})|^2 = \langle \chi \rangle + 2X_1(\underline{R}), \tag{3.28}$$

where $\langle \chi \rangle = \log |E_0(\underline{R})|^2$, and

$$\begin{aligned} \langle \chi^2 \rangle - \langle \chi \rangle^2 &= 4 \left\langle X_1^2 \right\rangle \\ &= 2\left[ \left\langle |X|^2 \right\rangle + \mathrm{Re} \left\langle X^2 \right\rangle \right]. \end{aligned} \tag{3.29}$$

Thus, to evaluate either the phase variance or the log-intensity variance we need to compute only $\left\langle |X|^2 \right\rangle$ and $\left\langle X^2 \right\rangle$. These calculations are carried out in Appendix A. The result is

$$\left\langle |X(\underline{R})|^2 \right\rangle = r_e^2 \lambda^2 \int_{R'}^{R''} dx \int d^2k_\perp \ F(0,\underline{k}_\perp) \tag{3.30}$$

$$\left\langle X^2(\underline{R}) \right\rangle = - r_e^2 \lambda^2 \int_{R'}^{R''} dx \int d^2k_\perp \ F(0,\underline{k}_\perp) \exp(i\underline{k}_\perp^2 / qA) \ , \tag{3.31}$$

where $A \equiv R/x(R-x)$ is the wave curvature, R'-R" is the distance traversed in the layer, and $k_\perp$ is the component of the spatial wave number perpendicular to the direction of transmission.

A detailed discussion of the nature of $\langle |X(\underline{R})|^2 \rangle$ and $\langle X^2(\underline{R}) \rangle$ is given in Chapter 10 of Ref. [23]. The quantity $\langle |X(\underline{R})|^2 \rangle$ in (3.30) is the same result as obtained by computing $X(\underline{R})$ in geometrical optics (cf. 3.26). In fact, $\langle |X(\underline{R})|^2 \rangle$ is the same as $\Phi^2$ in geometrical optics. The quantity $\langle X^2(\underline{R}) \rangle$ in (3.31) is, however, different from the value obtained from a geometrical-optics calculation. The geometrical-optics result for $\langle X^2(\underline{R}) \rangle$ is obtained by expanding the exponential in (3.31) and replacing it by unity. This would correspond to the condition $k_\perp^2/qA \ll 1$ for all spatial wave numbers in the integration in (3.31). Let some typical $k_\perp$ be equal to $L^{-1}$ where L is the correlation length. Thus the condition for the validity of geometrical optics becomes $1/L^2 qA \ll 1$. Since $A^{-1} \sim R$ this condition is the same as the Fresnel condition $\Lambda \equiv (\sqrt{R/q}/L)^2 \ll 1$. In terms of (3.30) and (3.31), the phase variance is given by

$$\langle \phi^2 \rangle = r_e^2 \lambda^2 \int_{R"}^{R'} dx \int d^2 k_\perp \, F(0, \underline{k}_\perp) \tfrac{1}{2} [1 + \cos(k_\perp^2/qA)] \, . \qquad (3.32)$$

This is the Rytov result for the phase variance. For the geometry in Fig. 2 (3.32) can be written as

$$\langle \phi^2 \rangle = r_e^2 \lambda^2 \sec^2\theta \int_0^{\Delta L} dz \int dk_x dk_y F(k_x, k_y, -\tan\theta\cos\phi k_x - \tan\theta\sin\phi k_y)$$

$$\times \tfrac{1}{2}[+\cos\{\frac{k^2 + k_y^2 + \tan^2\theta \, (k_x\cos\phi + k_y\sin\phi)^2}{qA}\}] \; ; \qquad R'-R" = \Delta L\sec\theta \, . \qquad (3.33)$$

The geometric-optics result for $\langle \phi^2 \rangle$ corresponds to replacing the cosine term in brackets by unity. This approximation is valid if and only if the argument of the cosine can be neglected for all relevant values of $k_x$ and $k_y$. To examine the result (3.33) further, we replace the wave curvature function by its value $\bar{A}$ in the middle of the scattering layer. (For a scattering layer at 300 km from the receiver and a layer thickness of 50 km and a satellite height of 1000 km, A varies between $4.5 \times 10^{-3}$ km$^{-1}$ and $5.0 \times 10^{-3}$ km$^{-1}$ and may be approximated by some average value without introducing major errors.) In this approximation,

$$\langle \phi^2 \rangle = r_e^2 \lambda^2 \sec^2\theta \Delta L \int dk_x dk_y F(k_x, k_y, -\tan\theta\cos\phi k_x - \tan\theta\sin\phi k_y) \times \frac{1}{2}\left[1+\cos\left\{\frac{k_x^2+k_y^2+\tan^2\theta(k_x\cos\phi+k_y\sin\phi)^2}{q\bar{A}}\right\}\right]. \tag{3.34}$$

We are now in a position to incorporate the anisotropy of the ionosphere into our expressions.

Using the generalized anisotropy model of Rino and Fremouw[33,34] we may rewrite (3.34) as

$$\langle \phi^2 \rangle = r_e^2 \lambda^2 \sec^2\phi \Delta L \; ab \left\langle \Delta N_e^2 \right\rangle M_1', \tag{3.35}$$

$$M_1' = \frac{1}{(2\pi)^2} \int dk_x dk_y Q([Ak_x^2 + Bk_x k_y + Ck_y^2]^{1/2}) \times \frac{1}{2}\left[1+\cos\left\{\frac{k_x^2+k_y^2+\tan^2\theta(k_x\cos\phi + k_y\sin\phi)^2}{q\bar{A}}\right\}\right] \tag{3.36}$$

where A, B and C are functions of the anisotropy scale factors a, b and the anisotropy angles (see Fig. 4). Eq. (3.36) can be simplified by a diagonalizing transformation followed by integration over the angular variables. The

details are given in Appendix B. The result is

$$M_1' = \frac{1}{4\sqrt{AC - B^2/4}} \int dk k Q(k)[1 + \cos(k^2\gamma_1) J_0(k^2\gamma_2)], \tag{3.37}$$

where $\gamma_1$ and $\gamma_2$ are defined in Appendix B. The limits of integration over the spatial frequencies must be determined once again by the nature of the data processing. As per our earlier discussion, we set the outer scale to $q_e$ and the inner scale to $\infty$ to obtain

$$M_1' = \frac{1}{4\sqrt{AC - B^2/4}} \int_{q_e}^{\infty} dk k Q(k)[1 + \cos(k^2\gamma_1) J_0(k^2\gamma_2)]. \tag{3.38}$$

Thus the phase variance $\langle \phi^2 \rangle$ in the Rytov approximation is given by

$$\langle \phi^2 \rangle = \frac{r_e^2 \lambda^2 \sec^2 \theta \Delta L \; ab \; \langle \Delta N_e^2 \rangle}{4\pi (AC - B^2/4)^{1/2}} \int_{q_e}^{\infty} dk k Q(k)[1 + \cos(k^2\gamma_1) J_0(k^2\gamma_2)]. \tag{3.39}$$

Substituting the expression $Q(k)$ from (3.8) and scaling out $q_e$, we obtain

$$\langle \phi^2 \rangle = B \int_1^{\infty} \frac{dk \, k}{(q_0^2/q_e^2 + k^2)^{\nu+1/2}} \left\{ 1 + \cos(k^2 q_e^2 \gamma_1) J_0(k^2 q_e^2 \gamma_2) \right\} \tag{3.40}$$

where

$$B = \frac{r_e^2 \lambda^2 \Delta L \sec^2\theta \; ab \langle \Delta N_e^2 \rangle \; q_e^{-2\nu+1}}{4\pi (AC - B^2/4)^{1/2}} \tag{3.41}$$

Similarly, using (3.29), (3.30), and (3.31), the variance of log-intensity is given by

$$\langle \iota^2 \rangle - \langle \iota \rangle^2 = 2\,B \int_1^\infty \frac{dk\ k}{(q_0^2/q_e^2 + k^2)^{\nu+\frac{1}{2}}} \left\{ 1 - \cos(k^2 q_e^2 \gamma_1) J_0(k^2 q_e^2 \gamma_2) \right\} \quad (3.42)$$

Note the relative sign in the bracketed terms in (3.40) and (3.42).

## 4. DATA ANALYSIS

Ionospheric scintillation data obtained from satellite observations have been analyzed by several workers. Of particular interest to this section is the work of Crane[6,7], Rino[12] and Fremouw[13]. Crane has presented an extensive discussion of the data gathered from the U.S. Navy Navigational System Satellites (NNSS) at Millstone. Details of the receiving system at the Millstone Radar Facility is described in his review article[7]. Two phase coherent sources at 150 and 400 MHz were used. This enabled the elimination of phase shifts introduced due to the satellite motion. Crane analyses of the phase and amplitude scintillation through the evaluation of such measures as the phase variance $\langle \phi^2 \rangle$, log-intensity variance $\langle \iota^2 \rangle - \langle \iota \rangle^2$ $(=4\langle \chi^2 \rangle \equiv \left(\frac{\ln 10}{10}\right)^2 \sigma_\chi^2)$ and the intensity scintillation $S_4$. Rino has carried out a similar analysis for the wide band P76-5 satellite data. The accumulation and processing of the wide band satellite data is described in the paper of Fremouw et al.[9] The wide band satellite used coherent signals in the VHF, UHF, the L-Band and the S-Band. Observations were made in Ancon (Peru), Kwajalein (Marshall Islands), Poker Flat (Alaska) and Stanford (California). Rino and Fremouw present detailed analysis of $\sigma_\phi$ and $S_4$ for each of these observations stations.

(i) Weak vs Strong Scatter Theories.

The main point we wish to discuss is the theoretical models used by these researchers to analyze the data. Rino[12,37] concludes in his 1979 papers that a major part, if not the whole, of ionospheric scattering phenomena might be described by the Born approximation. His conclusion rests on the following two arguments. First, in the case of the ionosphere the outer scale is sufficiently large that $q_0[\lambda/\bar{A}]^{\frac{1}{2}}$, where $A^{-1} = \frac{(R-x)x}{R}$ is the reduced

height, is much smaller than unity. Second, for the ionospheric scattering, Rumsey's intensity randomization parameter U, which is essentially the average square intensity, is much smaller than unity. It is argued that these two factors are sufficient to justify the application of the Born approximation theory to data. Fremouw[13] has also given support to this argument in his 1980 paper where he concluded that U~0.1 for ionospheric scattering.

Crane's analysis[7] of the Millstone data points to a somewhat different conclusion. Crane compares the amplitude scintillation data to both Born and Rytov approximation results. In the Rytov calculation, the appropriate measure is $\langle X_1^2 \rangle$, (cf. 3.29) proportional to the variance of the log-intensity. In the Born approximation, he uses the intensity scintillation $S_4$. His comparison of theory and data indicates that neither Born nor Rytov agrees with the data in its entirety. Simulatenous observations of $\sigma_\chi$ and $S_4$ clearly shows saturation behavior beyond $\sigma_{\chi,150}$ = 5.56 dB and $S_{4,150}$ values above 0·8. Thus there does appear in ionospheric scattering data, points that cannot be fitted by either Rytov or Born approximation. Even Fremouw's $S_4$- $\sigma_\phi$ scatter diagram (see fig. 11) indicates such points with large values of $S_4$ and clearly a weak scatter theory is not likely to be correct for these data points. The fit of Rino[12] for passes such as Ancon 32-06 and Poker Flat 12-24 show deviations when $S_4$ values are large particularly around the edges of the pass. Also, the scintillation observed at Poker Flat invariably shows enhanced scintillation at points in and around the middle of the pass. This enhancement is distinct from the gradual enhancement observed at the edges, see for example, for the Poker Flat Pass 12-24 (Fig. 5), Pass (6-14) (Fig. 6) and our theoretical Rytov curves for Pass 6-39 (Figs. 17, 18). There are portions of the pass for which $S_4$ or $\chi^2$

clearly exceeds the limits of the weak scatter theory and saturation sets in. Hence, the weak scatter predictions are much larger than the data. In such regions there is no alternative except to use strong scatter theory.

(ii) Born vs. Rytov Approximation

Even in regions where $S_4$ is small the question arises as to whether the Born or the Rytov approximation is to be used. Crane[7] compares both approximations to data and favours the Rytov approximation (see Fig. 7). The Born approximation results for $S_{4,150}$ ranging from 0.2 to 0.4 lie below the data and those ranging from 0.8 to 1 lie above the data. The scatter of the data around theory is above the one dB limit whereas the scatter is less in the Rytov fit. It appears from this analysis that the Rytov fit is better. The phase variance calculations that we have carried out also raises some questions about the Born approximation. The Born approximation result for the phase as derived by Rino is the same as the geometric optics results given by

$$\langle \phi^2 \rangle_B = \langle |X|^2 \rangle \tag{4.1}$$

where $\langle |X|^2 \rangle$ is given by (3.3).

The Rytov approximation result is given by

$$\langle \phi^2 \rangle_{R_y} = 1/2\left[\langle |X|^2 \rangle - \mathrm{Re}\langle X^2 \rangle\right] \tag{4.2}$$

where $\langle X^2 \rangle$ is given by (3.31). These two results are equal if the outer scale is so large that for a significant part of the integration in (3.31) $k_\perp$ is essentially zero, i.e., diffraction effects due to the large scales are negligible and dominate the contributions to $\langle \phi^2 \rangle$. In ionospheric scattering the outer scale is not the relevant scale. As explained in

Sec. 2, limits of integration of the spectral function in (3.30) and (3.31) are set by the detrender and is some scale $q_e$ which may be much smaller than the outer scale cut-off $q_0$. Thus in the integration in (3.31) it may not be correct to approximate the exponential by unity. To examine these differences closely, we have computed the ratio of the phase variance in the Rytov approximation to that in the Born approximation. From (3.39) this ratio can be seen to be

$$\frac{\langle \phi^2 \rangle_{Ry}}{\langle \phi^2 \rangle_B} = \frac{\int_{q_e}^{\infty} dk\ k\ Q(k) \left\{ 1 + \cos\ (k^2 \gamma_1)\ J_0(k^2 \gamma_2) \right\}}{2 \int_{q_e}^{\infty} dk\ k\ Q(k)} \quad . \qquad (4.3)$$

The computation has been carried out for the Kwajalein Pass 22-13 and the Poker Flat Pass 6-39 (See Figs. 8, 9, 10). A rather interesting conclusion emerges from this comparison. For the Poker Flat case there is very little difference between the Rytov and Born results for sheet-like irregularity ratios of 10:10:1 and 40:40:1. However, there is a maximum of 10% difference for irregularities with ratios 40:10:1 i.e., those that are intermediate between rods and sheets. Thus for the usually accepted sheet-like model for the irregularities the Born approximation is close to the Rytov results. In the Kwajalein case irregularities are rod-like and there is significant difference between Born and Rytov results. For an irregularity ratio 10:1:1 there is a maximum deviation of about 15% which appears quite sharply within the satellite pass (see Fig. 10). For higher irregularity ratios of 40:1:1 and 100:1:1 the deviations become more pronounced. The 100:1:1 result lies slightly below 40:1:1 but has a very similar shape. All these results point to the conclusion that there is significant difference between Born and Rytov results in the equatorial stations which again imply that the

diffraction effects may not be negligible. A reason why these effects are more pronounced in the equatorial station compared to the polar station is the rod-like nature of the irregularities in the former compared to the sheet-like irregularity in the latter. For the two passes we considered (and also for other typical passes of the P 76-5 satellite) the x-component of the satellite velocity (in the geomagnetic north-south direction) is ten times larger than the y- component (in the east-west direction). When the irregularities are sheet-like the effective velocity $V_e$ is still dominated by the $V_x$ component and is quite large. The effective outer scale $q_e = L_e^{-1} = (V_e\tau_e)^{-1}$ (See Sec. 2) is then quite small and diffraction effects are small. When the irregularities are rod-like, the effective velocity is considerably reduced (it is only about 15% of $V_x$). In this case the effective outer scale $V_e$ is large and the diffraction effects are non-negligible.

There is experimental evidence to indicate that diffraction effects are lowering the phase variance in equatorial stations. Fremouw examines the $S_4$-$\sigma_\phi$ diagram for several passes (see Fig. 11). He finds that the ratio $S_4$-$\sigma_\phi$ is consistently higher in equatorial stations as opposed to polar stations. Fremouw seeks an explanation for this effect in such factors as the incidence angle $\Theta$, ionospheric anisotrophy, source motion etc. He concludes that it is the course motion coupled with the effect of detrending on phase scintillation that explains this difference in the ratio $S_4/\sigma_\phi$. Our calcuations would not only support this view but also strengthen it. Fremouw's viewpoint is that there is more diffraction introduced because of the source motion and the detrender cutoffs in the equatorial case compared to the polar case. He has, however, examined the diffraction effects in $S_4$ only and not included it in his $\sigma_\phi$ calculation which is essentially a

geometric-optics calculation. When we carry out the calculation in the Rytov approximation $\sigma_\phi$ decreases because of diffraction. Thus the increase of the ratio $S_4/\sigma_\phi$ arises not only because of the increase of $S_4$ but also because of the decrease of $\sigma_\phi$ due to diffraction. The decrease in $\sigma_\phi$, as pointed out earlier, appears only in the Rytov approximation.

(iii) Rytov Calculations

To examine the sensitivity of the phase and intensity scintillation we have computed these quantities in the Rytov approximation for the Kwajalein Pass 22-13 and the Poker Flat Pass 6-39. For this purpose we have arbitrarily set the value of $\langle\phi^2\rangle$ to 0.2 in the middle of the pass. The variance of log-intensity is computed with the phase variance normalized to this value. We have chosen two values of the spectral index $\nu = 1.3$ and $\nu = 1.5$ which are representative of the values encountered in the ionospheric measurements. We first discuss the equatorial case. We have chosen three anisotrophy ratios 10:1:1. 40:1:1 and 100:1:1. The phase variance $\langle\phi^2\rangle$ monotonically increases for increasing anisotrophy. (See Figs. 12 & 13). It also increases smoothly towards the edges of the pass, an effect caused primarily by the $\sec\theta$ factor in (3.41). The calculated phase variance is not likely to be correct towards the edge of the pass if the corresponding log-intensity variance is high. Then the phase and the intensity should be given by the strong scatter formulae. Crane finds that experimentally this occurs at $\langle\chi^2\rangle - \langle\chi\rangle^2 \sim 1.2$. Since our normalization is arbitrary we cannot find from our graphs at what point the weak scatter approximations breakdown. Our calculations show that it is possible to distinguish anistropy ratio of 10:1:1 from 40:1:1 but the latter anisotropy yields results quite close to that of 100:1:1. Thus it is difficult to find accurate estimates of the

anisotropy ratios from $\langle\phi^2\rangle$ and $\langle\imath^2\rangle - \langle\imath\rangle^2$. These results are also quite insensitive to the spectral indices.

The Poker Flat pass exhibits a more complicated behavior. We have analyzed three anisotropy ratios 10:10:1, 40:10:1 and 40:40:1. The variance $\langle\phi^2\rangle$ is once again arbitrarily set to 0.2 slightly to the left of the middle of the pass. The most striking feature is the abrupt increase of the phase variance in the middle of the pass for all the anisotrophy ratios. This variation is in fact spurious and is caused by a very rapid variation in the azimuth. At these points the error bars on the measured velocities are very large. So, the computation of these data points is far from accurate. These data points appear at the top of each curve (see Fig. 16-18). Excluding these data points still leaves a jagged curve representing the phase and the intensity data. The intensity scintillation shows quite a bit of variation and the weak scatter theory probably does not apply at the scintillation peaks. In any case, the sharp increases observed in the intensity data (see Fig. 6) and our theoretical curves (Fig. 17, 18) argue against the exclusive use of the weak scatter theory.

## CONCLUSION

We summarize the major conclusions as follows.

1. Contrary to the claim of Rino[12] and Fremouw[13] the application of the weak scattering theory to the entire ionospheric data base is not justified. In both equatorial and polar stations, there appear data points for which the variance of the intensity $S_4$ is quite large. In polar stations such points appear when the signal trajectory lies transverse to the short axis. In equatorial stations high values of $S_4$ are encountered at the edges of the pass. Under such conditions a strong scatter theory should be used.

2. Even in regions where weak scatter theory is applicable, the Rytov approximation is preferable to the Born approximation for the phase calculations. This observation is consistent with Crane's analysis[7] of the Millstone data. In equatorial regions there is a very significant difference between the Rytov and Born approximation results indicating that the diffraction effects are non-negligible.

3. The diffraction effects reduce the phase variance and lead to smaller $\sigma_\phi$, an effect which is particularly pronounced for equatorial stations. The Rytov approximation partially accounts for these diffraction effects whereas the usual geometric optics calculation neglects them altogether. Thus for the same strength of electron density perturbations, $S_4/\sigma_\phi$ is larger in equatorial than in polar stations. This is another theoretical

reason that can be advanced to explain the enhancement in $S_4/\sigma_\phi$ observed by Fremouw[13] in equatorial stations compared to that in polar stations.

## REFERENCES


1. J.S. Hay, S.J. Parsons and J.W. Phillips, Nature, 158, 234, 1946.

2. G.G. Little and A. Maxwell, Phil. Mag. 42, 267, 1951.

3. H.G. Booker, Proc. IRE, 46, 298, 1958.

4. K.C. Yeh and G.W. Swenson, J. Res. Nat. Bur. Stand. Rad. Sci., 68D, 881, 1964.

5. J. Aarons, H.E. Whitney and R.S. Allen, Proc. IEEE 59, 159, 1971.

6. R.K. Crane, J. Geophys. Res. 81, 2041, 1976

7. R.K. Crane, Proc. IEEE, 65, 180, 1977.

8. E.J. Fremouw and H.F. Bates, Rad. Sci. 6, 863, 1971.

9. E.J. Fremouw, R.L. Leadabrand, R.C. Livingston, M.D. Cousins, C.L. Rino, B.C. Fair, and R.A. Long, Rad. Sci. 13, 167, 1978.

10. E.J. Fremouw, R.C. Livingston and D.A. Miller, J. Atmos. Terres. Phys. 42, 717, 1980.

11. R.C. Livingston, Rad. Sci. 15, 801, 1980.

12. C.L. Rino, Rad. Sci., 14, 1135, 1979.

13. E.J. Fremouw, J. Atmos. Terr. Res., 42, 775, 1980.

14. H.G. Booker, J.A. Ratcliffe and D.H. Shinn, Phil. Trans. Roy. Soc. A242, 579, 1950.

15. R.P. Mercier, Proc. Cambridge Phil. Soc., 58, 382, 1962.

16. B.H. Briggs and I.A. Parkin, J. Atmos. Terr. Phys., 25, 339, 1963.

17. V. Tatarski, The Effects of Turbulent Atmospheres on Wave Propogation, (National Technical Information Services. Springfield, Virginia, 1971).

18. A. Prokhorov, F. Bunkin, K. Gochelashvily and V. Shishov, Proc. IEEE 63, 790, 1975.

19. R.L. Fante, Proc. IEEE 63, 1669, 1975.

20. A. Ishimaru, Rad. Sci., 10, 52, 1975.

21. V.H. Rumsey, Rad. Sci., 10, 107, 1975.

22. R. Dashen, J. Math. Phys., 20, 804, 1979

23. S.M. Flatte, ed., Sound Transmission Through A Fluctuating Ocean (Cambridge University Press, New York, 1979).

24. C.L. Rino and E.J. Fremouw, Rad. Sci., 8, 223, 1973.

25. H.E. Whitney, J. Aarons, R.S. Allen and D.R. Seemann, Rad. Sci., 7, 1095, 1972.

26. Y.N. Barbanenkov, Y.A. Kravtsov, S.M. Rytov and V.I. Tatarski, Sov. Phys. Uspekhi, 12, 551, 1971.

27a. V. Seshadri and B.J. West, La Jolla Institute Technical Report LJI-TN-80-107.

b. La Jolla Institute Technical Report LJI-TN-81-136.

c. La Jolla Institute Technical Report LJI-R-81-161.

28. J.W. Strohbehn and S.F. Clifford, IEEE Trans. Antennas Propagat. AP-15, 416, 1967.

29. E. Collett and R. Alferness, J. Opt. Soc. Amer. 62, 529, 1972.

30. H.G. Booker and J.A. Ferguson, J. Atmos. Terr. Phys. 40, 803, 1978.

31. L.S. Taylor, J. Math. Phys. 13, 590, 1972.

32. de Wolf D.A., J. Opt. Soc. Amer., 63, 171, 1973.

33. C.L. Rino and E.J. Fremouw, J. Atmos. and Terr. Phys., 39, 859, 1977.

34. D.G. Singleton, J. Atm. Terr. Phys., 32, 789, 1970.

35. C.G. Callan and F. Zachariasen, Stanford Res. Institute Technical Report No. JSR-73-10 (April 1974) unpublished.

36. W.H. Munk and F. Zachariasen, J. Acoust. Soc. Am., 59, 818, 1976.

37. C.L. Rino, Rad. Sci., 14, 1157, 1979.

## Appendix A

### Evaluation of $\langle|X^2|\rangle$ and $\langle X^2\rangle$

Let us first evaluate $\langle|X|^2\rangle$. Using (3.23), (3.24) and the definition of $R(\underline{r})$ from (3.3), we obtain:

$$\langle|X(\underline{R})|^2\rangle = r_e^2 \iint d^3r' d^3r'' \frac{|\underline{R}|^2}{|\underline{R}-\underline{r}'||\underline{r}'||\underline{R}-\underline{r}''||\underline{r}''|} \times R(\underline{r}'-\underline{r}'')\exp[iq\{|\underline{R}-\underline{r}'| + |\underline{r}'| - |\underline{R}-\underline{r}''| - |\underline{r}''|\}]. \tag{A.1}$$

The integral in (A.1) can be evaluated using a stationary phase methods. The stationary path is along a straight line from the origin to the point $\underline{R}$. To see this we choose $\underline{R}$ along the z-direction. Introducing the difference variables

$$\underline{r}' - \underline{r}'' = \underline{y}\ , \quad \tfrac{1}{2}(\underline{r}' + \underline{r}'') = \underline{x}, \tag{A.2}$$

we obtain $\left.\begin{matrix}|\underline{R}-\underline{r}'| \\ |\underline{R}-\underline{r}''|\end{matrix}\right\} = \left|\underline{R} - \underline{x} \mp \tfrac{1}{2}\underline{y}\right|$

$$= \sqrt{(R - x_k)^2 + (x_i \pm \tfrac{1}{2}y_i)^2 + (x_j \pm \tfrac{1}{2}y_j)^2}$$

$$\left.\begin{matrix}|\underline{r}'| \\ |\underline{r}''|\end{matrix}\right\} \approx \sqrt{x_k^2 + (x_i \pm \tfrac{1}{2}y_i)^2 + (x_j \pm \tfrac{1}{2}y_j)^2}, \tag{A.3}$$

where $(x_i, x_j, x_k)$ are the components of $\underline{x}$ and $y_k$ has been neglected. Thus the exponent in (A.1) reduces to $\exp iq\{(x_iy_i + x_jy_j)\frac{R}{x_k(R - x_k)}\}$.

In terms of these new variables (A.1) can be rewritten as

$$\langle|X(\underline{R})|^2\rangle = r_e^2 \int d^3y \int d^3x \frac{R^2}{(R-x_k)^2 x_k^2}$$

$$\times \exp\left\{iq(x_iy_i+x_jy_j)\frac{R}{x_k(R-x_k)}\right\} \tag{A.4}$$

An integration over $dx_i\, dx_j$ yields

$$\iint dx_i dx_j\, e^{iq\{(x_iy_i + x_jy_j)\frac{R}{x_k(R - x_k)}\}}$$

$$= \left(\frac{2\pi}{q}\right)^2 \left[\frac{x_k(R - x_k)}{R}\right]^2 \delta(y_i)\delta(y_j). \tag{A.5}$$

Substituting the result (A.5) in (A.4), we arrive at

$$\langle|X(\underline{R})|^2\rangle = r_e^2 \lambda^2 \int_{R''}^{R'} dx \int dy_{\shortparallel}\, R_2(y_{\shortparallel}), \tag{A.6}$$

where $y_{\shortparallel}$ is the integration variable parallel to the straight-line path and $(R' - R'')$ is the distance traversed in the layer. In terms of the frequency spectrum of $R_{\Delta Ne}$, we can rewrite (A.6) as

$$\langle|X(\underline{R})|^2\rangle = r_e^2 \lambda^2 \int_0^{R'} dx \int d^2k_{\perp}\, F(0,\underline{k}_{\perp}) \tag{A.7}$$

An entirely analogous stationary-phase calculation can be carried out for evaluating $\langle X^2(\underline{R})\rangle$. From (3.7) and (3.8) we obtain

$$\langle X^2(\underline{R})\rangle = r_e^2 \int d^3r'' \, d^3r' \frac{|\underline{R}|^2}{|\underline{R} - \underline{r}'||\underline{R} - \underline{r}''||\underline{r}'||\underline{r}''|} R(\underline{r}' - \underline{r}'')$$

$$\times \exp iq\{|\underline{R} - \underline{r}'| + |\underline{r}'| + |\underline{R} - \underline{r}''| + |\underline{r}''| - 2|\underline{R}|\}. \qquad (A.8)$$

Once again, the stationary path is the straight line from the origin to the point $\underline{R}$. Expanding the exponential as before,

$$|\underline{R} - \underline{r}'| + |\underline{r}'| + |\underline{R} - \underline{r}''| + |\underline{r}''| - 2|\underline{R}|$$

$$= \{(x_i^2 + y_i^2/4) + (x_j^2 + y_j^2/4)\} \times \{\frac{1}{x_k} + \frac{1}{(R - x_k)}\}. \qquad (A.9)$$

(A.8) can be rewritten

$$\langle X^2(\underline{R})\rangle \simeq r_e^2 \int_{R''}^{R'} \frac{dx_k R^2}{(R - x_k)^2 x_k^2} \int d^3y R(y) \int dx_i dx_j$$

$$\exp[iq\{x_i^2 + y_i^2/4 + x_j^2 + y_j^2/4\}\{\frac{1}{x_k} + \frac{1}{R - x_k}\}]. \qquad (A.10)$$

Performing the Gaussian integration , we obtain

$$\langle X^2(\underline{R})\rangle \simeq \frac{ir_e^2\pi}{q} \int_{R''}^{R'} \frac{dx_k R}{(R - x_k)x_k} \int d^2 y_\perp \, dy_\parallel R(y_\parallel, \underline{y}_\perp)$$

$$\exp[iq\frac{y_\perp^2}{4}\{\frac{1}{x_k} + \frac{1}{R - x_k}\}], \qquad (A.11)$$

where $y_\perp^2 = y_i^2 + y_j^2$. Introducing the Fourier transform of $R(\underline{r})$ as before,

$$\langle X^2(\underline{R})\rangle = -\frac{4\pi^2 r_e^2}{q^2}\int_{R''}^{R'} dx \int d^2k_\perp F(0,\underline{k}_\perp)\exp[iqk_\perp^2(\frac{x(R-x)}{R})], \qquad (A.12)$$

where the subscript k on $x_k$ has been dropped.

## Appendix B

Consider the following transformation,

$$\begin{pmatrix} k'_x \\ k'_y \end{pmatrix} = \begin{pmatrix} 1 & B/2A \\ 0 & 1 \end{pmatrix} \begin{pmatrix} kx \\ ky \end{pmatrix} , \tag{B.1}$$

which diagonalizes the quadratic form of the argument of Q in (3.17). In terms of the variables $k'_x$, $k'_y$ the integral over the second term in (3.15) $\equiv$ I is

$$I=\frac{1}{2\pi}\int dk'_x dk'_y Q(Ak'^2_x+(C-B^2/4A)k'^2_y)\cos\left(\frac{\alpha_1 k'^2_x+\alpha_2 k'_x k'_y+\alpha_3 k'^2_y}{q\bar{A}}\right) \tag{B.2}$$

where

$$\alpha_1 = 1 + \tan^2\theta \cos^2\phi$$

$$\alpha_2 = 2 \tan^2\theta \sin\phi \cos\phi - \frac{B}{A}(1 + \tan^2\theta \cos^2\phi)$$

$$\alpha_3 = \frac{B^2}{4A^2}(1 + \tan^2\theta \cos^2\phi) - \frac{B}{A} \tan^2\theta \sin\phi \cos\phi$$

$$+ (1 + \tan^2\theta \sin^2\phi). \tag{B.3}$$

Introducing the transformations

$$k_x'' = \sqrt{A}k_x' \qquad k_y'' = \sqrt{C - B^2/4A}\, k_y' \tag{B.4}$$

$$k_x'' = k\cos\theta \qquad k_y'' = k\sin\theta$$

successfully, we obtain

$$I = \frac{1}{2\pi}(AC - B^2/4)^{-1/2} \iint dk''k''Q(k'') \times \int_0^{2\pi} d\theta \cos\left[(\gamma_1 + \gamma_2\cos(2\theta - \phi))k^2\right] , \tag{B.5}$$

where

$$\gamma_1 = \frac{1}{2q\bar{A}}\left(\frac{\alpha_1}{A} + \frac{\alpha_3}{C - B^2/4A}\right)$$

$$\gamma_2 = \frac{1}{2q\bar{A}}\left[\left(\frac{\alpha_1}{A} - \frac{\alpha_3}{C - B^2/4A}\right)^2 + \frac{\alpha_2^2}{C - B^2/4A}\right]^{1/2}$$

$$\tan^{-1}\phi = \frac{\alpha_2 A\sqrt{C - B^2/4A}}{\alpha_1(C - B^2/4A) - \alpha_3 A} .$$

Performing the integration over $\theta$, we arrive at

$$I = \frac{1}{\sqrt{AC - B^2/4}} \int \cos(k^2\gamma_1) J_0(k^2\gamma_2) Q(k) k dk. \tag{B.7}$$

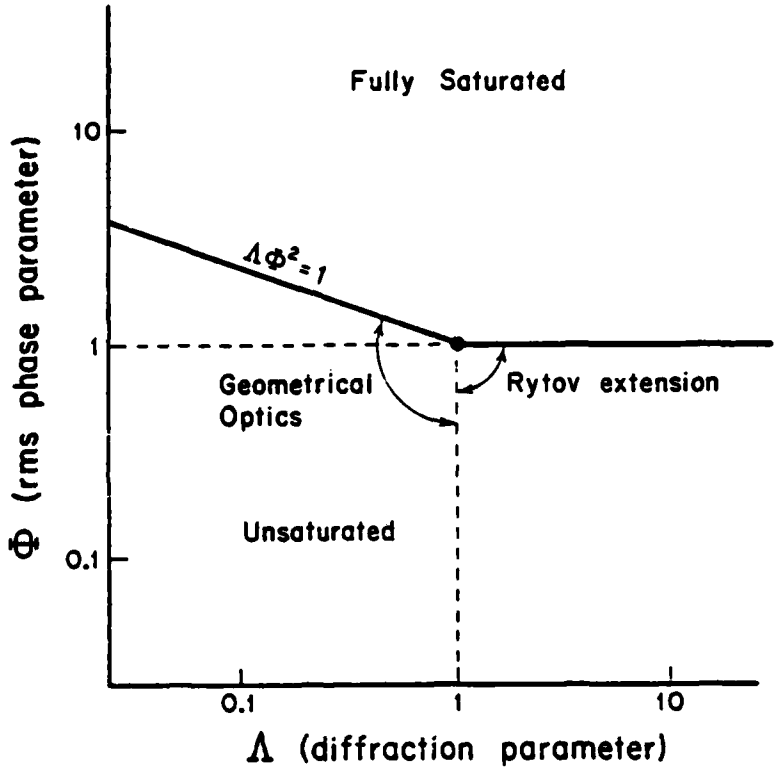
Fully Saturated
10
1
0.1
$\Lambda\Phi^2=1$
Geometrical Optics
Rytov extension
Unsaturated
Φ (rms phase parameter)
0.1
1
10
Λ (diffraction parameter)

Figure 1.

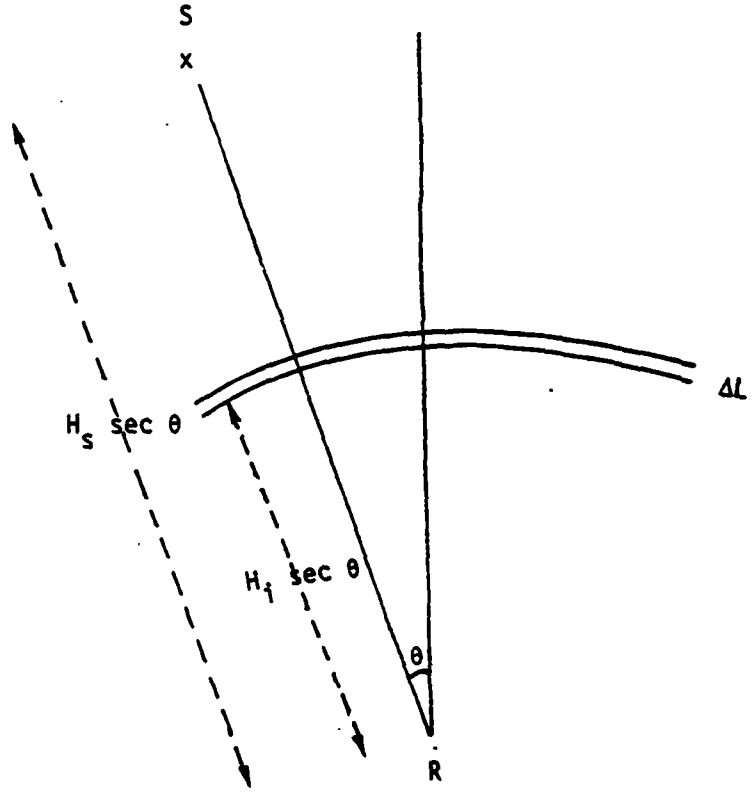


FIGURE 2: Source-Receiver geometry. θ is the angle of incidence with respect to zenith; $\theta_s$ is the scattering angle.

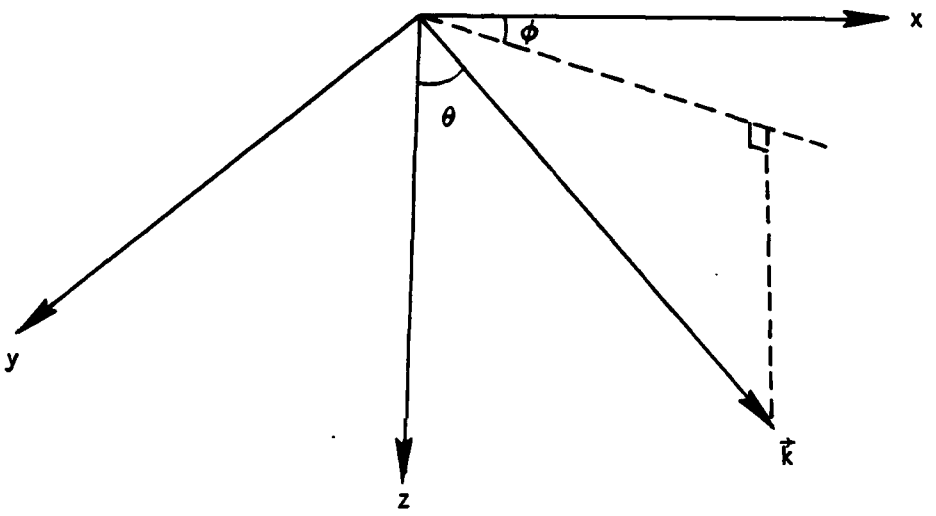


FIGURE 3: Wave Propagation Geometry: The propagation vector is at an angle $\theta$ w•r•t the z-axis and its projection in the xy plane is at angle $\phi$ w•r•t the x-axis.

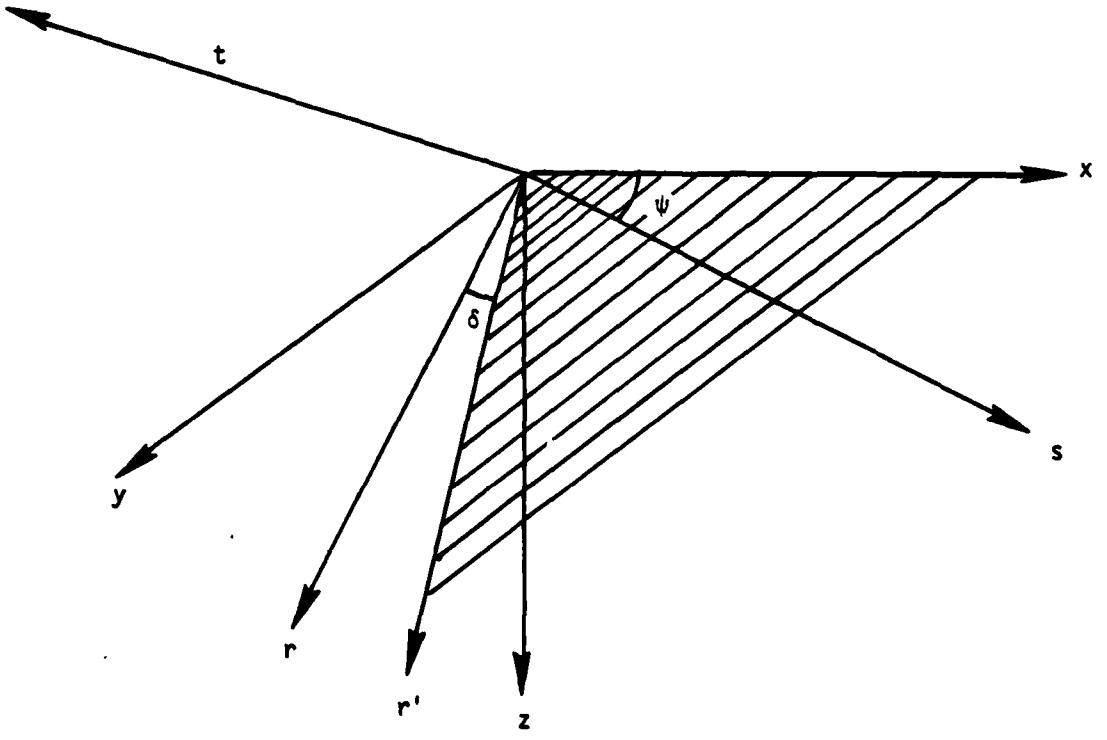


FIGURE 4: Ionospheric Anisotropy Geometry: s, r, t define an orthogonal coordinate system. s is along the magnetic field at an angle $\psi$ w•r•t the x-axis. The cross hatched region defines the plane of magnetic meridian. The other elongation axis r is at an angle $\delta$ w•r•t the plane of the magnetic meridian.

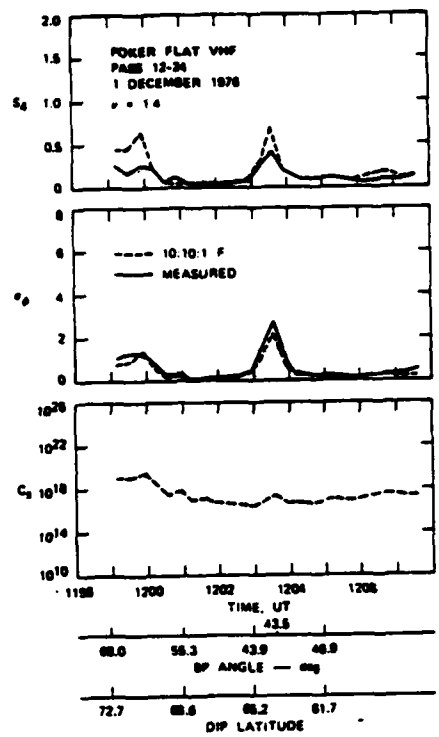


FIGURE 5: Data from Poker Flat pass 12-24 showing isolated geometrical enhancement attributed to sheetlike irregularities. (reproduced from C. L. Rino, Rad. Sci. 14, 1135 (1979)).

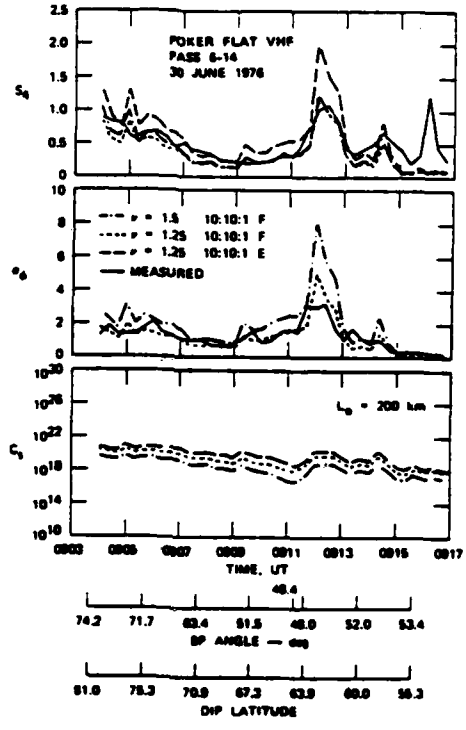


FIGURE 6: Data from Poker Flat pass 6-14 together with theoretical curves showing evidence of height change. (reproduced from C. L. Rino, Rad. Sci. 14, 1135 (1979)).

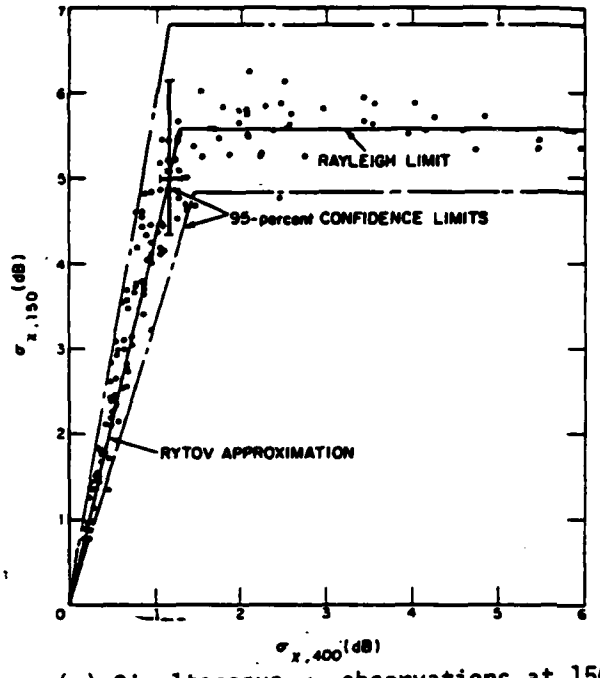


(a) Simultaneous $\sigma_\chi$ observations at 150 and 400 MHz.

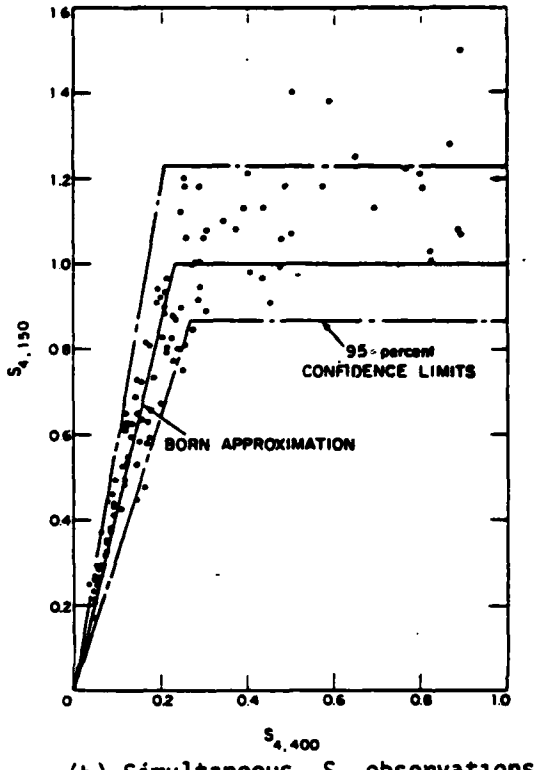


(b) Simultaneous $S_4$ observations at 150 and 400 MHz.

FIGURE 7: Reproduced from R. K. Crane, J. Geo. Phys. Res. 81, 2041, (1976).

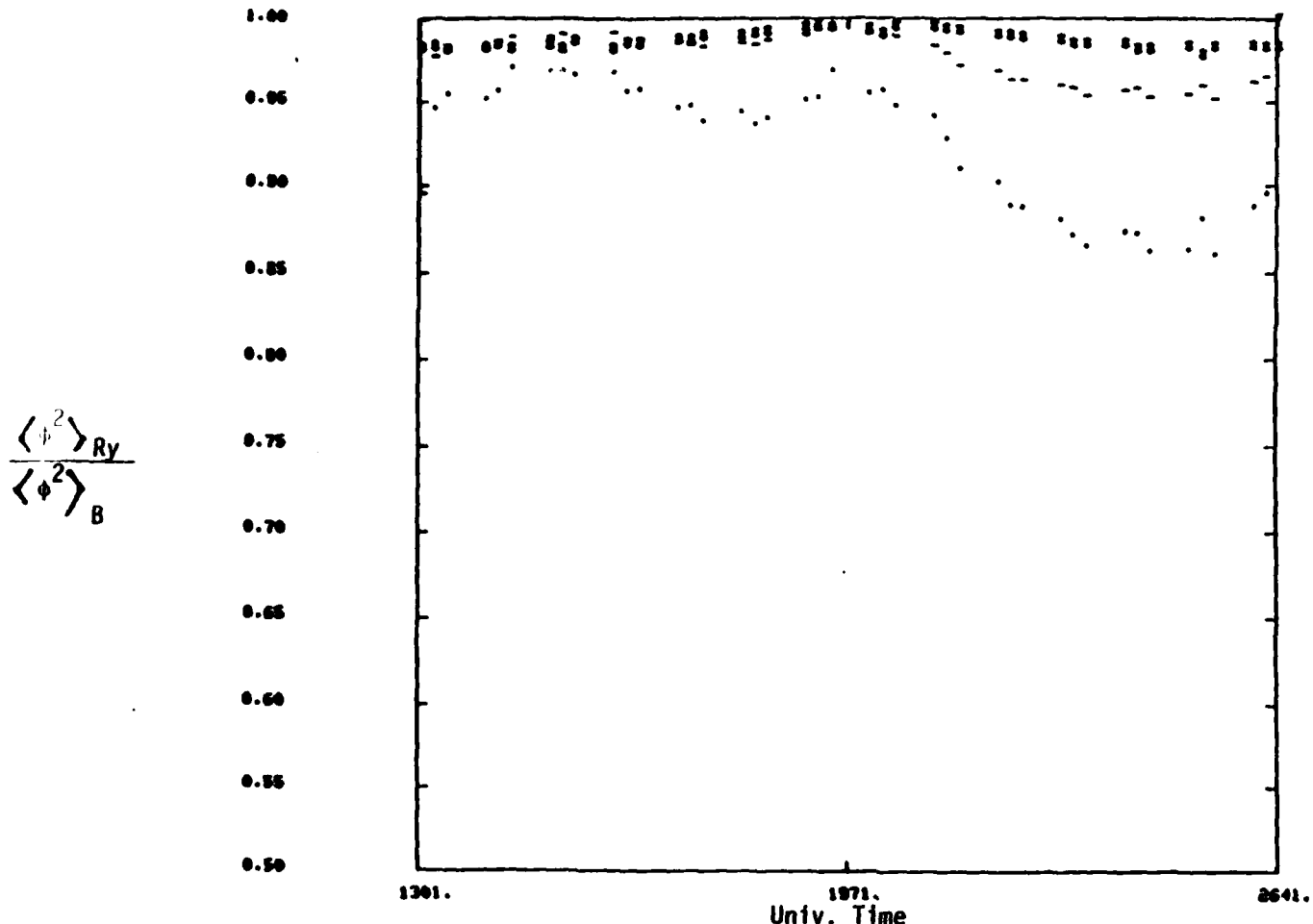


FIGURE 8: Ratio of phase variance computed in the Rytov and Born approximations for Poker Flat Pass 6-39 with $\nu$=1.3 and asymmetry ratios *** 10:10:1, ...40:10:1 and ---40:40:1.

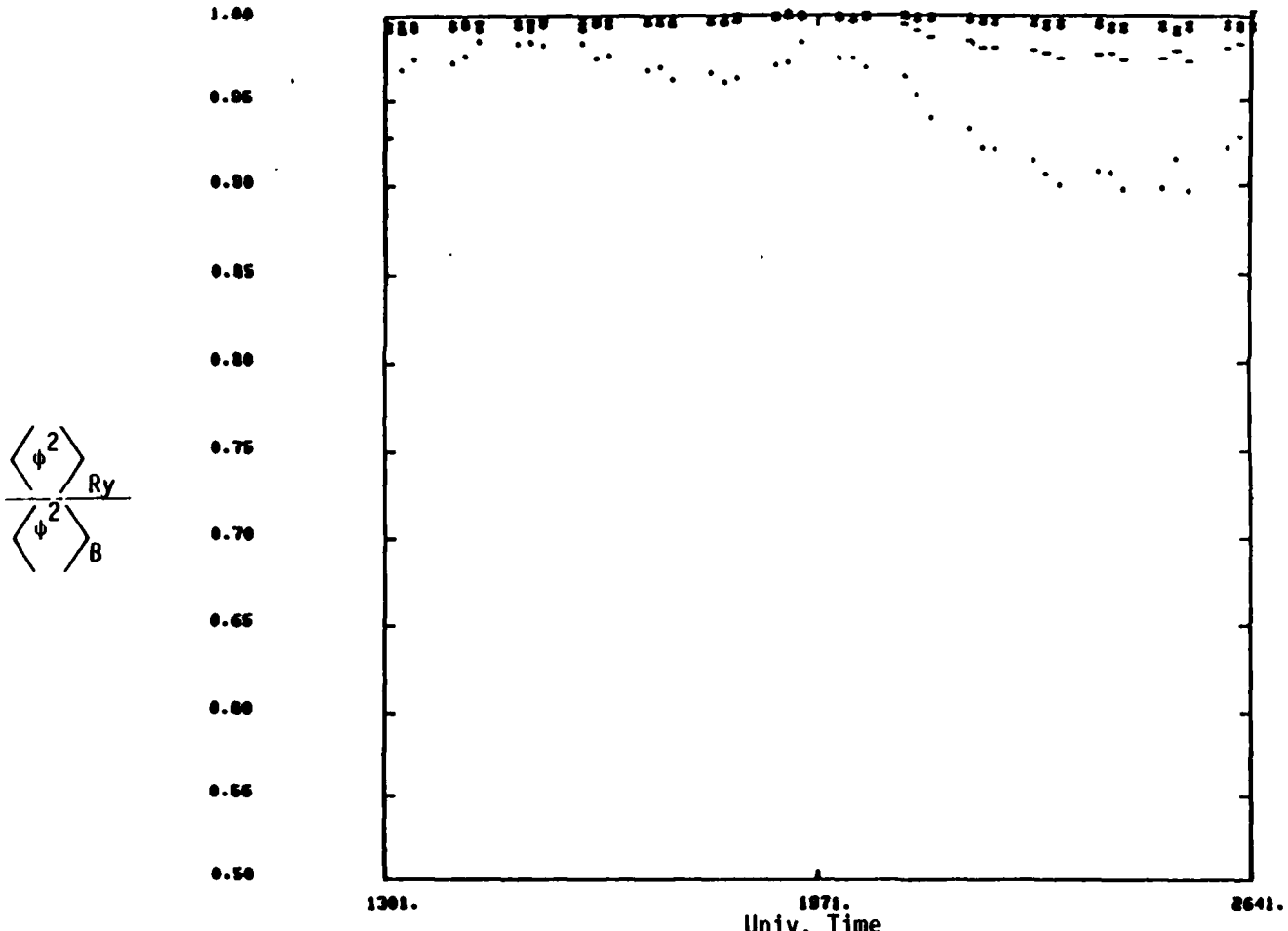


FIGURE 9: Ratio of phase variance computed in the Rytov and Born approximations for Poker Flat Pass 6-39 with $\nu$=1.5 and asymmetry ratios ***10:10:1; ... 40:10:1 and ---40:40:1.

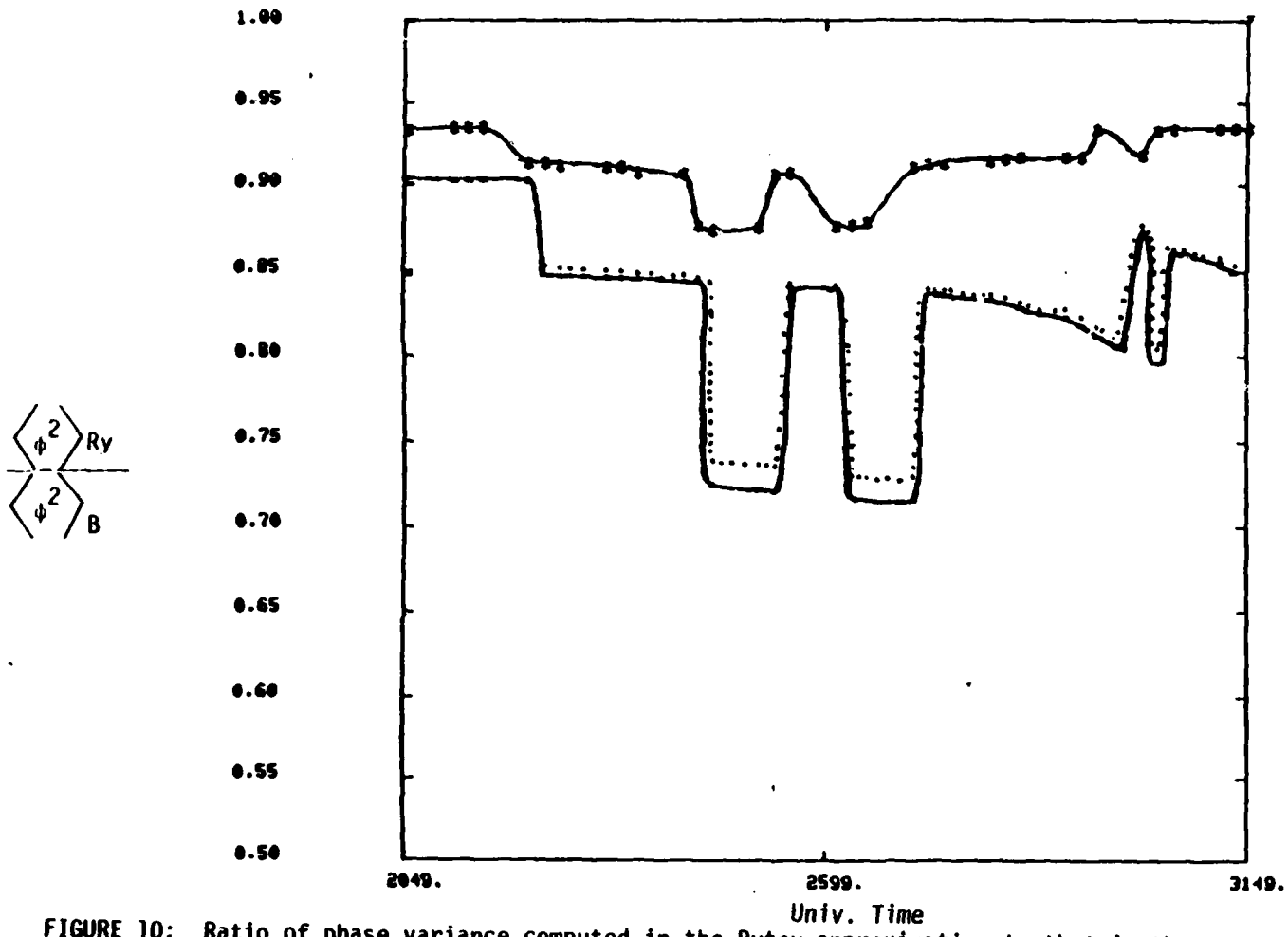


FIGURE 10: Ratio of phase variance computed in the Rytov approximation to that in the Born approximation for Kwajalein Pass 22-13 with $\nu$ =1.3 and 1.5 and asymmetry ratios ***10:1:1,...40:1:1 and ---100:1:1.

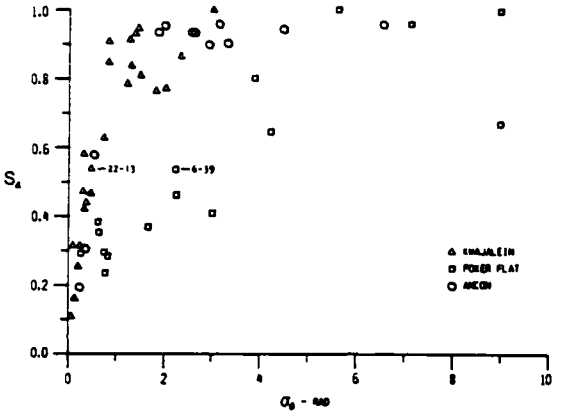


FIGURE 11: Scatter diagram of scintillation indices for intensity ($S_4$) and phase ($\sigma\phi$) for 50 VHF data segments ranging in length from 20 to 85s. Note consistency of pattern from two equatorial stations, Kwajalein and Ancon, and separate pattern formed by data from a high-latitude station, Poker Flat. (reproduced from E. J. Fremouw, J. Atmos. Res. 42, 775 (1980)).

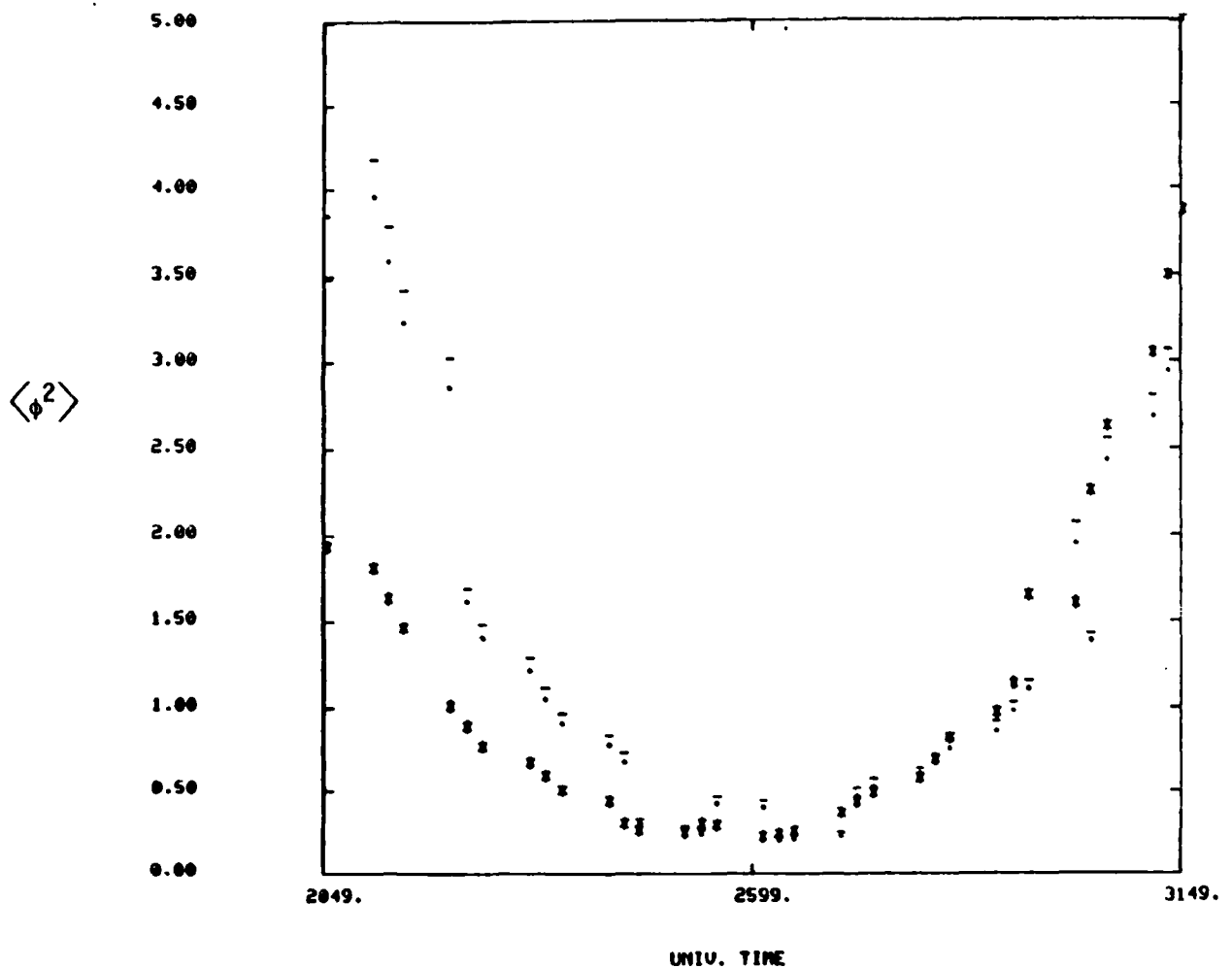


FIGURE 12: Mean square phase vs. univ. time for Kwajalein Pass 22-13 with $\nu$=1.3 and asymmetry ratios ***10:1:1, ...40:1:1 and ---100:1:1.

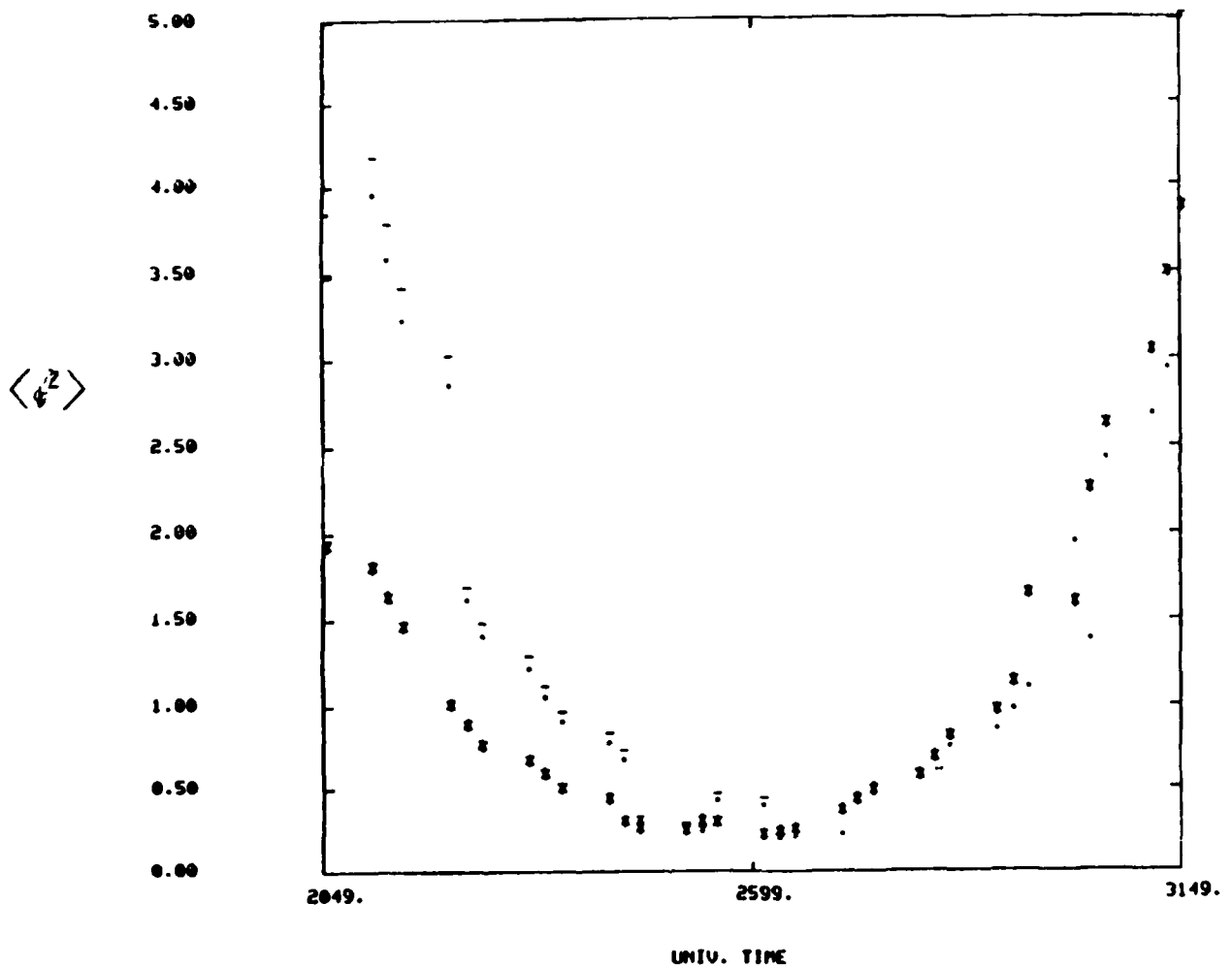


FIGURE 13: Mean square phase vs. univ. time for Kwajelein Pass 22-13 with $\nu$=1.5 and asymmetry ratios ***10:1:1, ...40:1:1 and ---100:1:1.

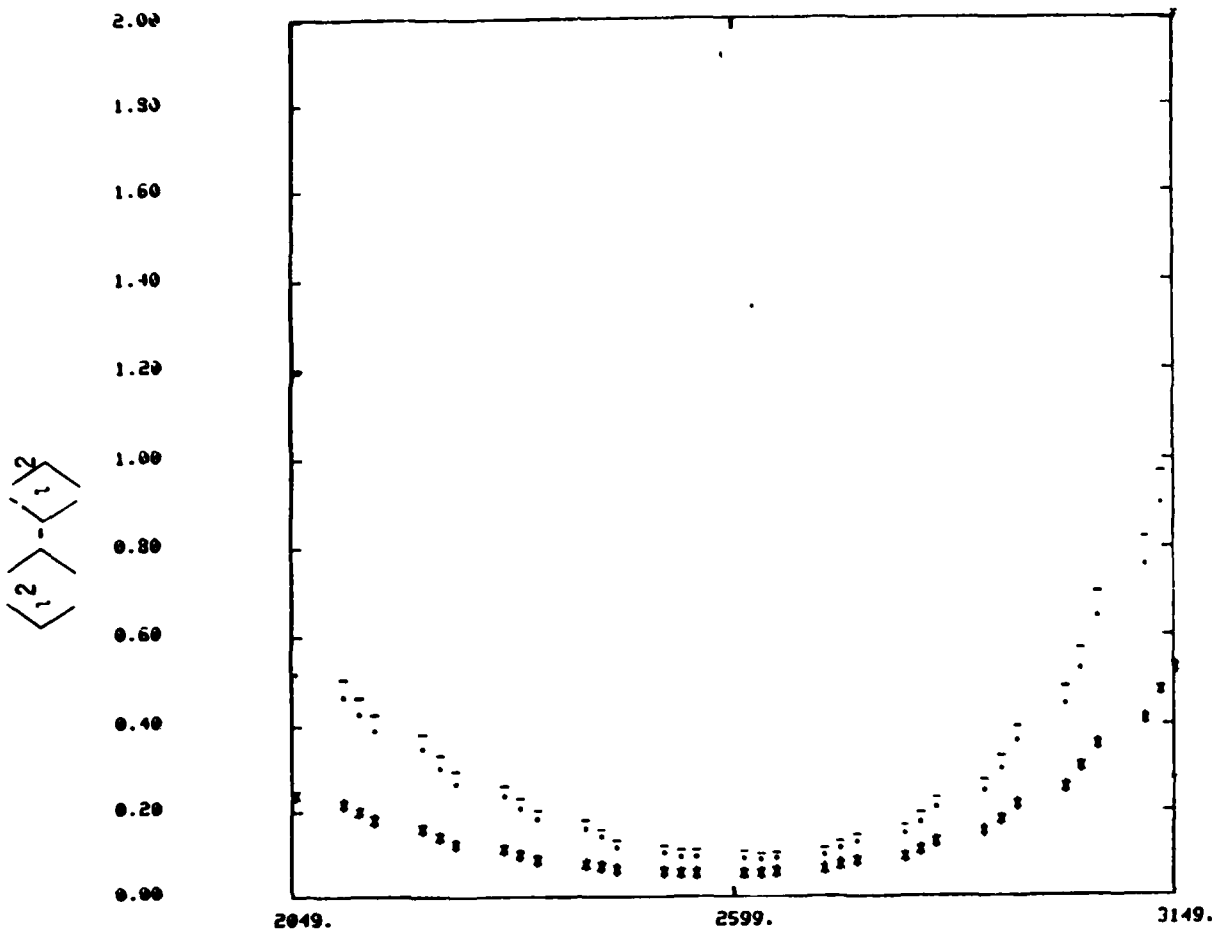


FIGURE 14: Variance of log intensity vs. univ. time for Kwajalein Pass 22-13 with $\nu$=1.3 and asymmetry ratios ***10:1:1, ...40:1:1 and ---100:1:1.

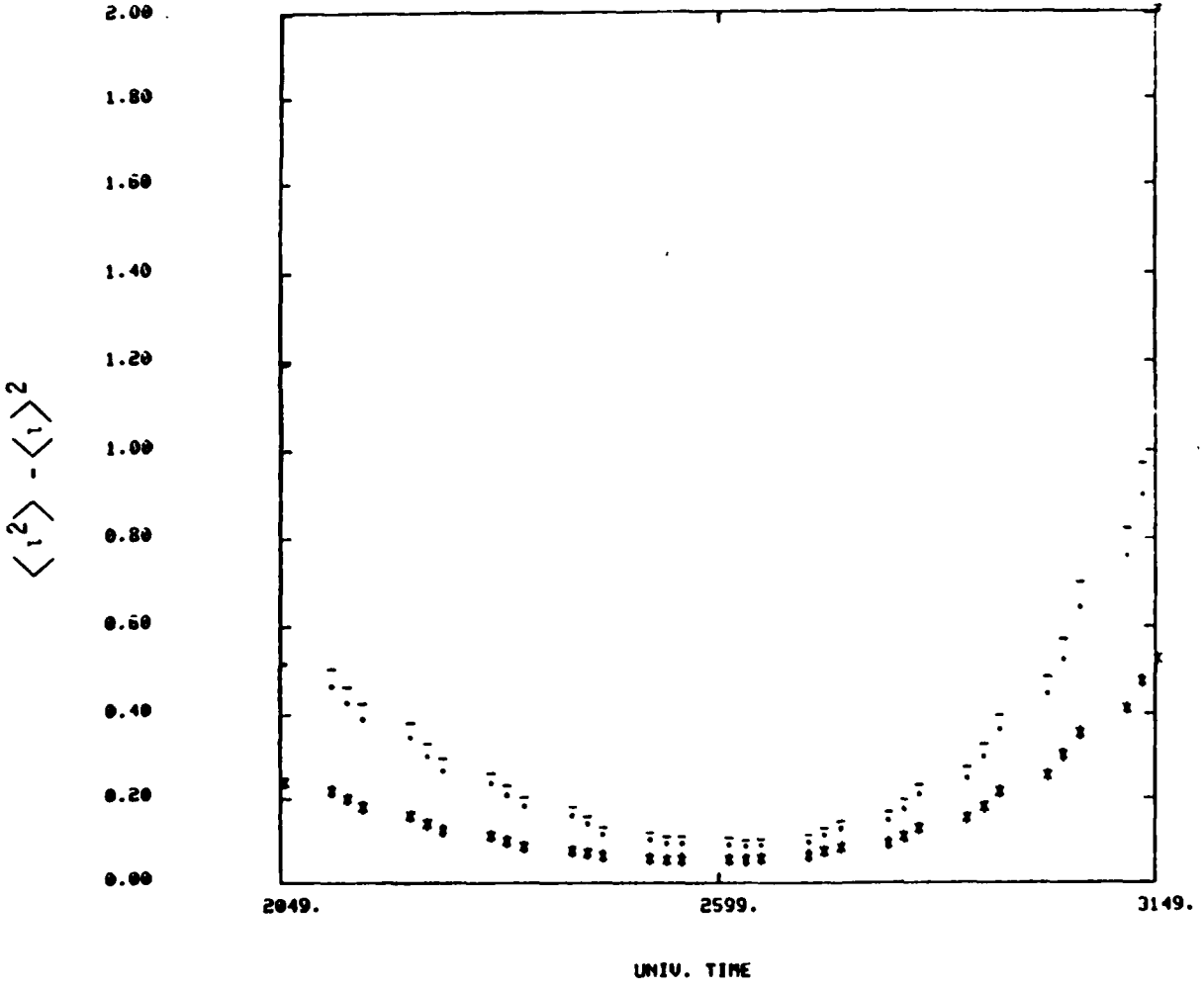


FIGURE 15: Variance of log intensity vs. univ. time for Kwajalein Pass 22-13 with $\nu$=1.5 and asymmetry ratios ***10:1:1, ...40:1:1 and ---100:1:1.

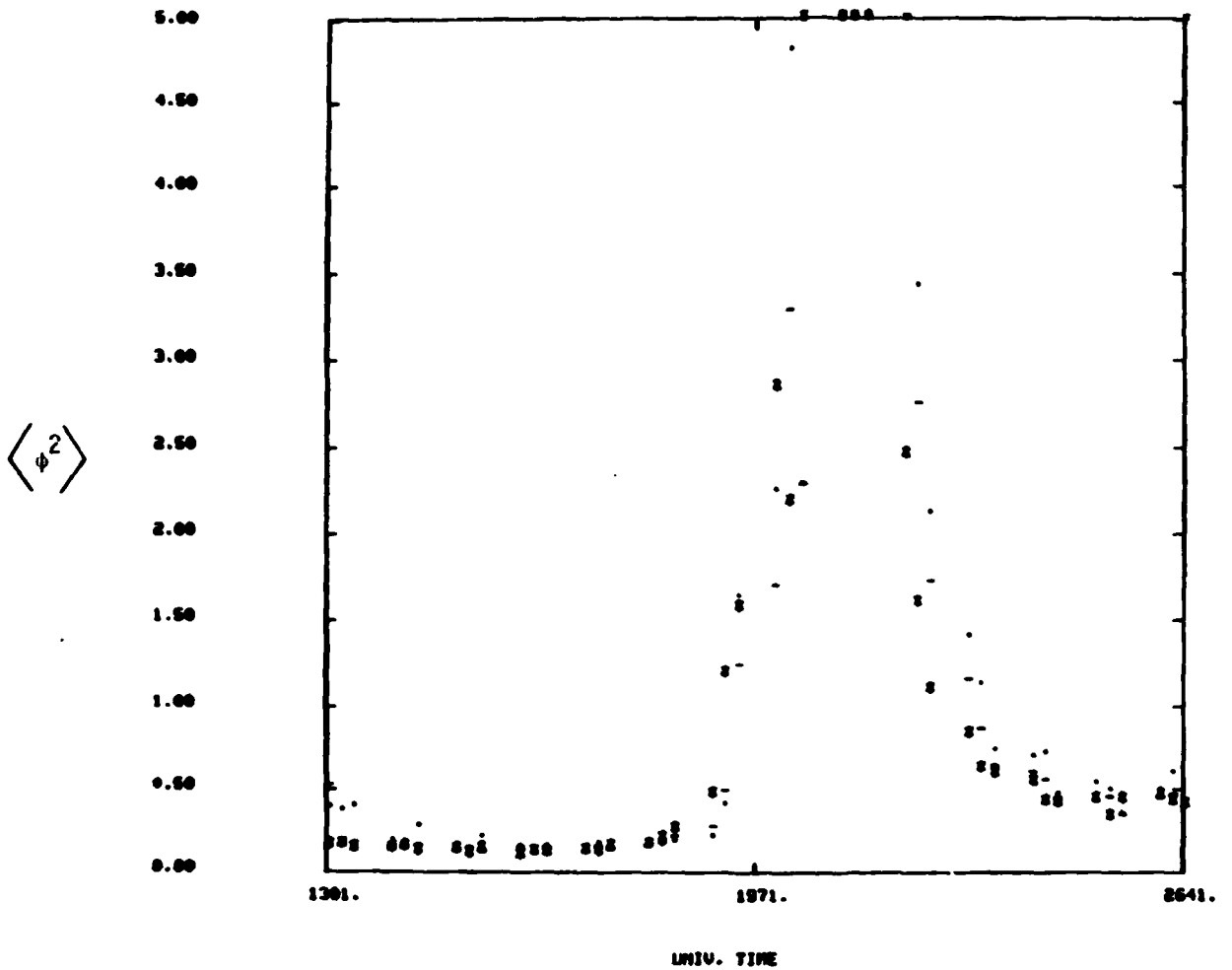


FIGURE 16: Mean square phase vs. univ. time for Poker Flat Pass 6-39 with ν=1.5 and asymmetry ratios ***10:10:1, ...40:10:1 and ---40:40:1.

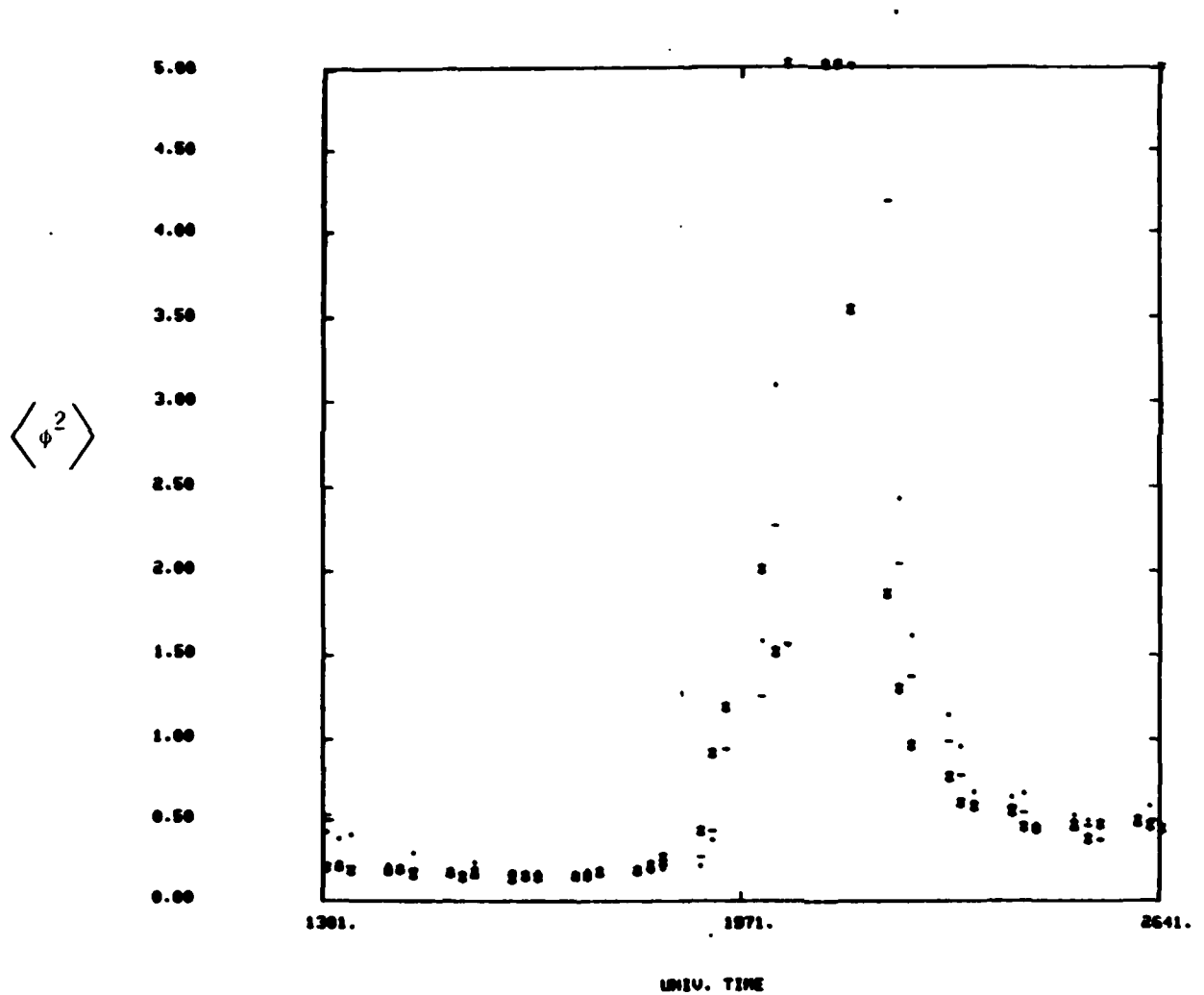


FIGURE 17: Mean square phase vs. univ. time for Poker Flat Pass 6-39 with $\nu$=1.3, and asymmetry ratios ***10:1:1, ...40:10:1 and ---40:40:1.

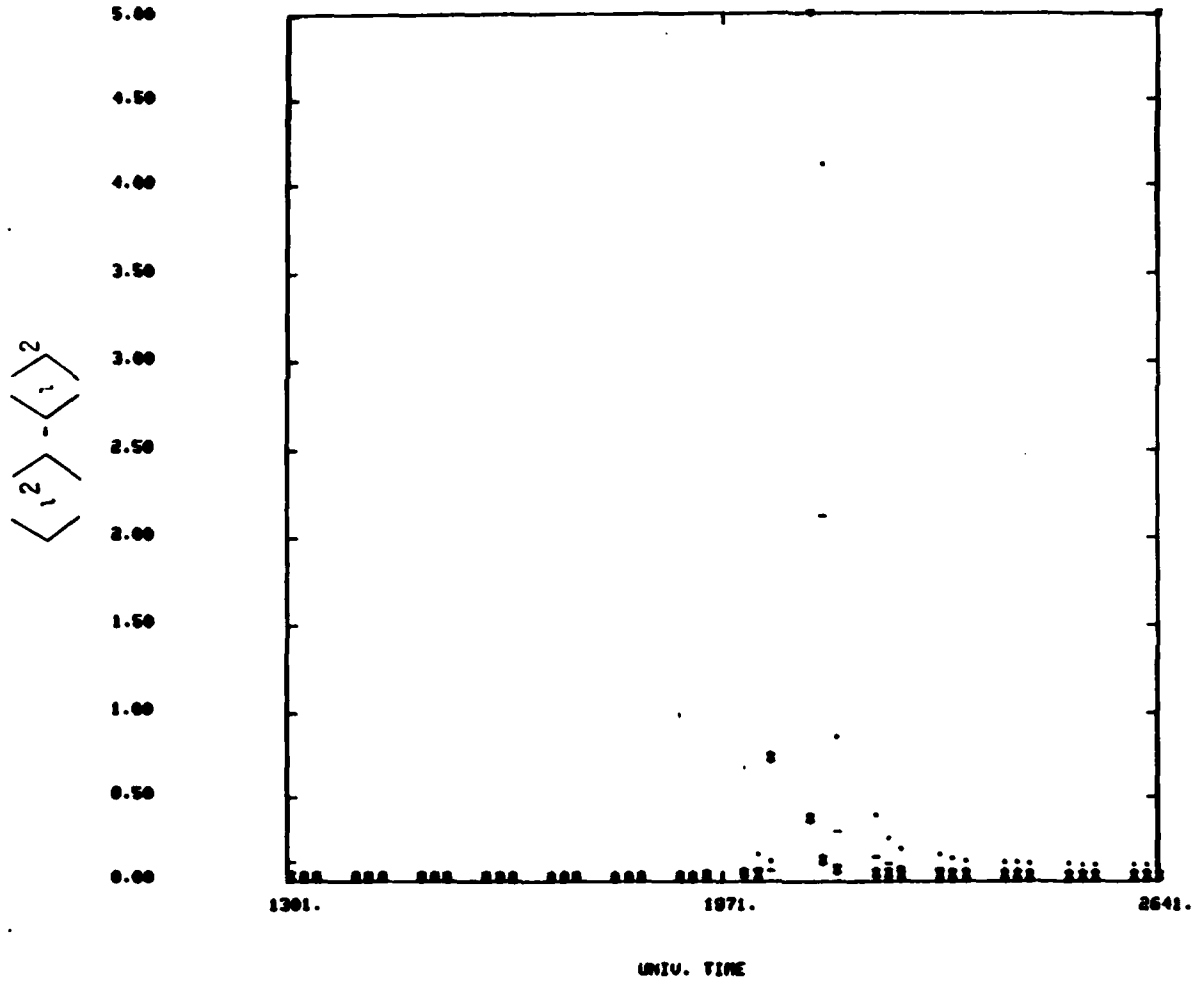


FIGURE 18: Variance of log of intensity vs. univ. time for Poker Flat Pass 6-39 with $\nu$=1.5 and asymmetry ratios ***10:10:1, ...40:10:1 and ---40:40:1

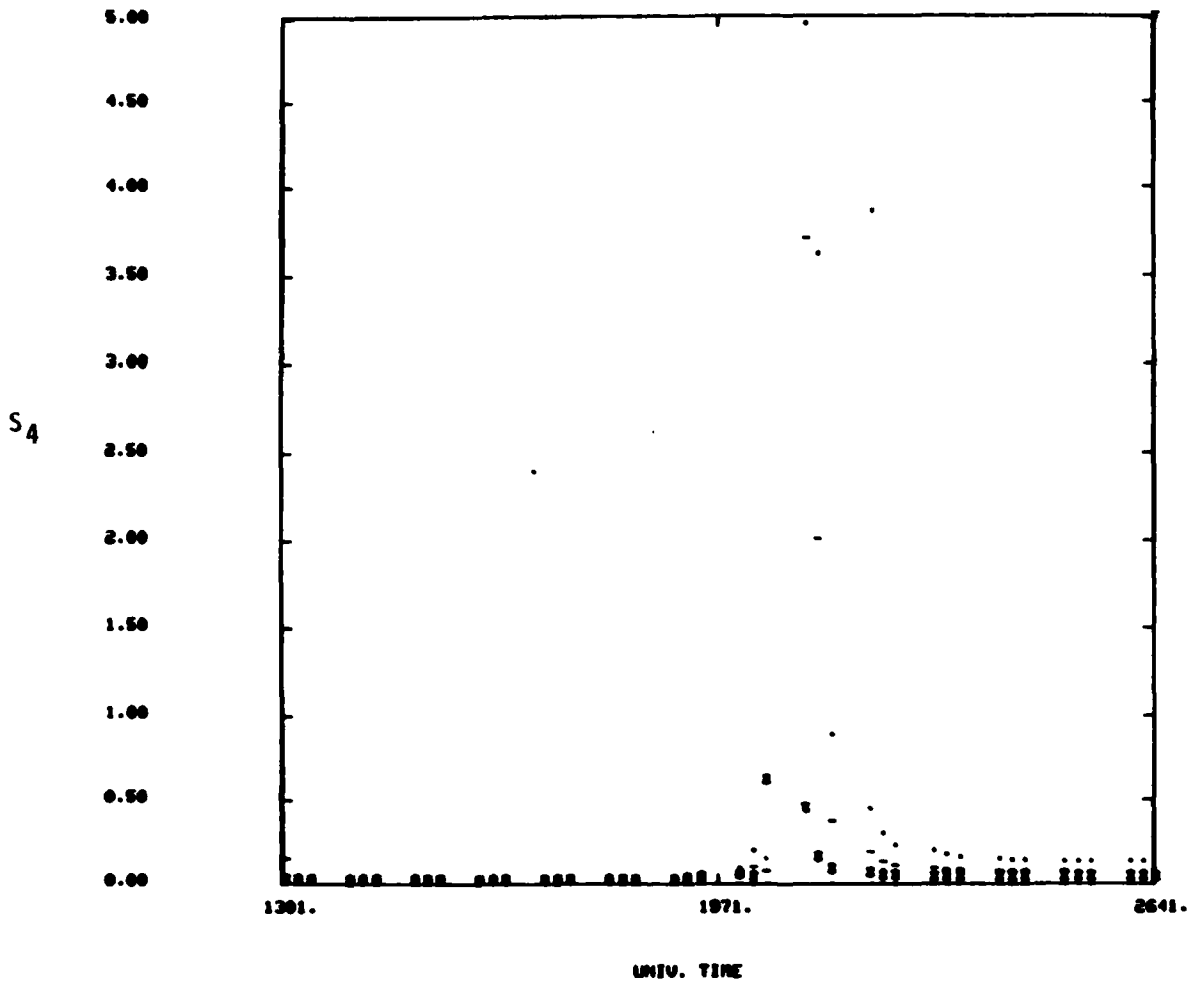


FIGURE 19: Variance of intensity vs. univ. time for Poker Flat Pass 6-39 for $\nu$=1.3 and asymmetry ratios ***10:10:1, ...40:10:1, ---40:40:1.

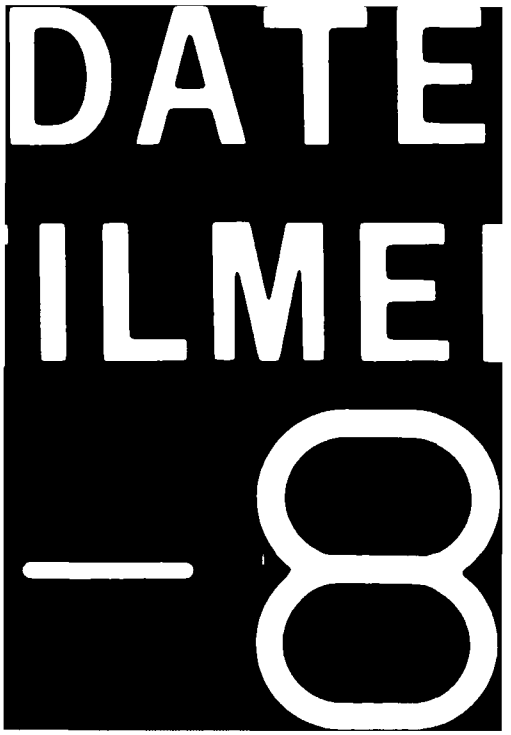
DATE
ILME
8